A review on the catalytic combustion of soot in Diesel particulate filters for automotive applications: From powder catalysts to structured reactors

Applied Catalysis A: General 509 (2016) 75–96

Contents lists available at ScienceDirect

Applied Catalysis A: General

journal homepage: www.elsevier.com/locate/apcata

Review

A review on the catalytic combustion of soot in Diesel particulate filters for automotive applications: From powder catalysts to structured reactors

Debora Fino*, Samir Bensaid, Marco Piumetti, Nunzio Russo

Department of Applied Science and Technology, Politecnico di Torino, Corso Duca degli Abruzzi 24, 10129 Turin, Italy

ARTICLE INFO

Article history:
Received 8 May 2015
Received in revised form 9 October 2015
Accepted 10 October 2015
Available online 22 October 2015

Keywords:
Soot oxidation
Diesel particulate filter
Modelling
Catalytic oxidation
Multifunctional traps

ABSTRACT

The current soot oxidation catalyst scenario has been reviewed, the main factors that affect the activity of powder catalysts have been highlighted and kinetic soot oxidation models have been examined. A critical review of recent advances in modelling approaches has also been presented in this work. The multiscale nature of DPFs lends itself to a hierarchical organization of models, over various orders of magnitude. Different observation scales (e.g., wall, channel, entire filter) have often been addressed with separate modelling approaches that are rarely connected to one another, mainly because of computational difficulties. Nevertheless, DPFs exhibit an intrinsic multi-scale complexity that is reflected by a trade-off between fine and large-scale phenomena. Consequently, the catalytic behavior of DPFs usually results in a non-linear combination of multi-scale phenomena.

Contents

* Corresponding author. Fax: +39 11 0904624.
E-mail address: debora.fino@polito.it (D. Fino).

http://dx.doi.org/10.1016/j.apcata.2015.10.016
0926-860X/

1. Introduction

Over the last few years, several exhaust gas aftertreatment technologies have been developed to reduce engine-out emissions. The latter are sources of the main outdoor air pollutants, that is, volatile organic compounds (VOCs), nitrogen oxides (NO_x) and particulate matter (PM), which is comprised of solid carbon (soot) and unburned carbonaceous compounds [1–3]. PM, in particular, is a major constituent of air pollution and is associated with respiratory and cardiovascular diseases as well as skin cell alterations [4]. EU estimates that "air pollution causes 100 million sick days and 350,000 premature deaths in Europe. Such health effects also have a heavy economic cost: air pollution from heavy goods vehicles (HGVs, mostly Diesel engine vehicles) alone costs EEA member countries €43–46 billion per year, making up almost half of the approximately €100 billion cost of air pollution from road transport" [5].

Consequently, recent legislation has introduced more stringent PM limits for vehicles (e.g., Europe = 0.005 g/km for PM from passenger cars since 2009) and has imposed the use of advanced catalytic technologies to satisfy the stated standards [1–3]. Among the different alternatives, the entrapment of particulates from exhaust gases by Diesel particulate filters (DPFs) has received much interest in recent years [6–11].

The soot that forms Diesel exhaust particulate can be burnt off at temperatures above 600 °C, whereas typical Diesel engine exhaust temperatures fall within the 200–500 °C range [10,11]. Therefore, oxidation catalysts are necessary to increase the oxidation rate of filter traps at low temperatures. Among the many oxidation catalysts developed since the 1980s, Ceria-based catalysts appear to be the most promising candidates for DPFs, since they exhibit excellent redox properties and are less expensive than noble metals [1]. Moreover, both the activity and stability of Ceria can be further improved with the addition of metals (e.g., rare-earth metals, transition metals, alkali and alkali-earth metals) to the crystal lattice. The main goal of soot combustion Ceria catalysts doping is to improve the thermal stability, although other physico-chemical properties could also change upon doping. Indeed, Diesel soot combustion is a demanding application due to the high temperatures achieved during combustion: the temperature inside the filter can increase up to ca. 1000 °C, and even more in specific hot spots, due to the highly exothermal soot combustion reaction.

DPFs are dynamic and complex systems, since the operating conditions vary over time, and different functionalities (=catalysis and filtration) are usually assembled on the same monolithic support, which is a demanding requirement in terms of space and cost. Moreover, the feasibility of soot combustion depends to a great extent on the catalyst–soot contact conditions, and it is therefore necessary to maximize the interaction between the soot particles and the catalyst, both of which are solid materials [12,13]. A pioneering approach to maximize the soot–catalyst contact was implemented by Peugeot-Citroën Société d'Automobiles (PSA) in early 2000s, whose key component is a Ce-fuel additive that was reliably implemented in several million vehicles up to now. PSA vehicles have an active on board additive system with its own tank-pump device that allows to dose the proper amount of Ce-fuel additive to the Diesel fuel. This metal organic compound in fuel leads to the formation of CeO_2 particles well embedded in the structure of diesel particulate, and thus in very good contact with the soot particles (intimate soot–catalyst contact). Therefore, lowers ignition temperatures can be reached by catalytic means, with the benefit of post-injected fuel savings. This system relies on an active regeneration strategy, activating timing adjustments to the fuel injection in the presence of high-pressure drops, which in turn increases the exhaust gas temperature, initiating the burning of the soot and regenerating, or clearing, the filter. Moreover, the catalyst stability for a PSA system plays a minor role with respect to catalytic materials dispersed onto the filter surface. Finally, since the Sulpur-content for on-road vehicle diesel fuels has gone down in Europe during the last decade (from 350 to 500 ppm to 10 ppm), the Cerium ash left over after the regeneration in PSA could be an active soot oxidation catalyst (e.g., in the form of Cerium oxide, Cerium nitrate and Cerium carbonate, instead of Cerium sulfate). On the other hand, unlike coated catalysts on the filter walls, its requires a trap over-sizing, in order to cope with the cerium oxide deposits' accumulation, and a dedicated storing and fueling strategy [14].

Other generations of fuel additives, which generate a particulate in which oxides of Fe (SATACEN) or of both Fe and Sr (OCTIMAX) remain embedded after combustion in the engine chambers. These solution proved to successfully lower the soot oxidation temperature, although not matching the balance point with exhaust gas temperatures, and thus still requiring active regeneration [15].

Computer modelling and simulation tools are now well established and allow catalysts and active sites to be described, as well as reaction intermediates and mechanisms. In addition, the knowledge of the processes that occur in the catalytic systems is a precondition for the reliability of the models over a wide range of operating conditions. In recent years, several ways of modelling exhaust after-treatment devices have been developed, since these are dynamic and complex chemical reactor systems in mass products [3,16]. In particular, a multiscale modelling approach for DPFs can be used to predict the operating conditions, in order to allow the optimization of operation strategies [16]. This may reduce testing costs and increase the durability of DPFs.

The multiscale complexity of DPFs requires a hierarchical organization of models, corresponding to different size scales (namely wall, channel and entire filter). These sub-models are classified according to their complexity and they should be combined to obtain an overall model [17].

This review considers the most important factors (i.e., the catalyst composition, the reaction mechanisms and the catalyst–soot contact) that can affect the activity of soot oxidation catalysts in laboratory-scale studies. In addition, advances in the modelling and simulation of DPFs, over the relevant length scales (from the atomic level to the macroscale) are discussed critically to reveal the complexity of DPFs at different observation scales.

2. Evaluation of catalytic soot oxidation activity

In laboratory-scale studies, the soot oxidation activity of powder catalysts is commonly assessed by means of temperature-programmed oxidation/combustion experiments (TPO/TPC). In a typical test, a proper amount of commercial carbon black (used as a model Diesel soot) and catalyst are loaded into a tubular quartz reactor and heated in an oxygen-containing atmosphere at a constant heating rate. The CO_x concentration profiles in the outlet gas are usually monitored by means of non-dispersive infrared (NDIR) gas analyzers. The CO_2 peak-temperature (generally denoted as T_m) is often used as an index of the catalytic activity. Other parameters that are used to study the activity include the CO and CO_2 peaks, the temperature for 50% soot conversion ($T_{50\%}$), and the onset temperature ($T_{10\%}$). However, the catalytic activity can also be investigated by means of a thermogravimetric (TG) analysis of catalyst–soot mixtures, using mass spectrometer or gas chromatograph detectors. This approach can be used to obtain useful information from the mass-temperature plots, such as the temperature of the maximum oxidation rate (T_0) and the temperature when soot oxidation begins (T_{onset}). In general, the main variables that influence the catalytic performances of soot oxidation catalysts are the soot composition, the soot–catalyst ratio, the type of catalyst–soot contact and the oxygen content in the feed mixture [18,19]. Unfortunately,

a great variation of these parameters can be found in literature, and it is therefore difficult to compare the activities of catalysts tested in different laboratories.

The use of carbon black as a soot surrogate is the best commercially available soot mimicking compound for catalysts screening, since real Diesel soot features are heterogeneous. However, available commercial soot samples (e.g., Printex-U) can present significant differences with Diesel soot, in terms of both microstructure and reactivity.

The physico-chemical features of real soot depend on several aspects, including the fuel and lubricating oil used, which contribute to the soluble organic fraction (SOF) content, the type of the engine and the operating conditions. Model and real soot differ in several aspects, as the amount and nature of ashes, since real soot incorporates the metals that Diesel fuels and lubricating oils contain. Moreover, real soot may come along with different amounts of unburned hydrocarbons (paraffin, aromatics and oxygenated compounds), which are related to the engine operating conditions, namely from 5 wt.%, for a loaded engine, to 60 wt.%, for an idle engine—thus being a complex aerosol better referred as particulate matter rather than soot, which comprises its carbonaceous fraction. On the other hand, model soot samples contain higher percentages of fixed carbon and lower percentages of volatile matter, ash and wetness than real soot samples. Therefore, Diesel soot combustion generally occurs at lower temperatures than those of commercial soot samples (e.g., Printex-U) for both the catalytic and non-catalytic cases, due to the higher amount of SOF on the soot particle surface which makes ignition easier [18].

However, the convenience of using Printex-U, as a substitute of Diesel soot, in catalyst screening experiments lies in the fact that conservative results are generally obtained with Printex-U, due to the absence of SOF in its composition. Differences of tens to a hundred of Celsius degrees can occur between soot oxidation temperatures of real and model soot, the latter exhibiting higher ones, at identical testing conditions [18], although these differences become less relevant in the presence of a catalyst. It is worth mentioning that discrepancies in reactivity are also related to the different crystalline structure of the carbonaceous fraction itself, depending on the nature of the fuel generating the particles, as later detailed.

Many soot-catalyst weight ratios have been reported in literature, with typical values ranging from 1/5 to 1/20. An increase in the soot-catalyst ratio beyond a certain value, at which the catalyst is no longer available to come into contact with the soot particles, will result in a shift in the oxidation temperatures to higher values. In other words, soot-catalyst ratios below ca. 1/10 do not generally influence the oxidation rate, while negative effects can be observed on catalytic activity for values above ca. 1/5 [18].

The contact between soot and catalyst plays a key role in solid–solid reactions, since the catalytic activity depends on the interaction between the two solids and the gas [20]. Two types of catalyst–soot contact conditions have been reported in the literature for laboratory-scale studies:

- a *"Loose" contact condition* is obtained by gently shaking the catalyst–soot mixture with a spatula. This procedure is sufficient to homogenize the mixture, but still allows the two solid phases to be put in contact loosely. Although the procedure is very short (1–2 min), the established contact leads to reproducible catalytic performances. Neeft et al. [20] observed that the contact between the catalyst and soot in a DPF is as loose as that of materials mixed roughly with a spatula.
- a *"Tight" contact condition* is usually prepared through ball milling (or in a mortar) to obtain close contact between the catalyst and soot. This method maximizes the number of contact points and, although it is less representative of the real contact conditions that occur in a catalytic trap, it is able to discriminate the morphologies better [21].

The composition of the feed also affects the catalytic activity. Oxygen is the reactive gas that is generally used to oxidize Diesel soot, even though NO_2 is a more powerful oxidant, and then higher oxidation activity can be obtained in a NO_x/O_2 atmosphere. The oxygen concentration in the gas mixture generally varies from 5% to 21%, with air being used most often [21–25]. Thus, under these conditions, oxygen is not the limiting reactant [22]. Moreover, the gas-hourly space velocity (GHSV) should be chosen so that the reaction occurs under a catalytic controlled regime: values from 20,000 to 60,000 h^{-1} are usually considered in the catalyst screening experiments for soot oxidation in DPFs, although above 100,000 h^{-1} occur in selected points of the engine map. As reported in [26], the operating conditions can summarize the complex regime of an engine: for a light-duty 2.0 l displacement Diesel engine, urban extra-urban and highway conditions have flue gas flow rates of nearly 120, 200 and 300 m^3/h, which correspond to 24,000, 40,000 and 60,000 h^{-1} (for a close-coupled filter volume of 5 l). More complete reactions (total oxidation processes) can be obtained under low flow rates, since the molecules have longer residence times.

3. Mobility of oxidizing species

Soot oxidation catalysts exhibit different activities, which depend on two main factors, namely the structural parameters and the reaction mechanisms: (i) the former (e.g., catalyst morphology, surface area, particle sizes, etc.) may affect the interaction between the soot and catalyst, which in turn could influence the utilization of the active sites; (ii) the latter (e.g., kinetic phenomena at solid surface) influence the reactivity of active sites [1,3].

It is worth noting that the active sites are not static at solid surfaces and may interact with each other through transport phenomena and surface flexibility [27–30]. This means that soot oxidation catalysts are dynamic entities that continuously adapt their physico-chemical properties under operating conditions.

Good activity cannot be attained under "loose" contact conditions, which are characterized by a low number of contact points, unless a certain mobility of the active species is achieved. It has been shown that a good understanding of the intrinsic reactivity of the "tight" contact combustion of soot over alkaline (Na, K, Cs) and alkaline-earth metal (Ca, Ba, Mg) oxides can be obtained [31]. The soot combustion reactivity has been found to be correlated to the electropositivity of metal ions, thus confirming the beneficial effect of the electron-donor elements. However, this correlation does not appear under "loose" contact conditions, where the mobility of some oxidizing species must be hypothesized to justify the activity orders. Hence, the oxidizing intermediates can be divided into two main categories [19]:

3.1. Long-distance oxidizing intermediates

3.1.1. NO_2 molecules

NO_2 molecules obtained by means of NO oxidation in the presence of O_2. Nitrogen oxides are present in Diesel exhaust fumes and several studies have reported that NO, in particular, has a beneficial effect on the catalyst activity of soot combustion, as it forms NO_2, which is a strong oxidant [32]. Thus, a direct reaction occurs between NO_2 and the carbon surface together with a simultaneous involvement of O_2 and NO_2 (denoted as the "NO_2-assisted mechanism"). This leads to a higher soot oxidation rate in the Diesel exhaust temperature window [1–3,9,32].

3.1.2. Catalytic molecules in the vapor phase

Catalytic molecules in the vapor phase obtained either by evaporation from a melting catalyst (e.g., Cu(oxy) chlorides from the Cu/Mo/V/Cl catalysts [33], as shown by Neeft et al. [20]) or via a reaction among several catalyst components (e.g., KI coupled to KVO_3, which releases I_2 vapors; Fino et al. [34]). However, this mechanism is practically inapplicable, as the catalyst is eventually destroyed and harmful compounds are released into the atmosphere.

3.1.3. Eutectic liquid compositions

Eutectic liquid compositions, which originate at temperatures within the Diesel exhaust range of interest (e.g., Cu/K/V/Cl catalysts, as shown by Serra et al. [35]; $CsSO_4{\cdot}V_2O_5$ catalysts by Setiabudi et al. [36]). This category is often accompanied by some volatility (e.g., Cu/K/V/Cl catalysts release chlorides) or solubility in water, or even the risk of the plugging of filter pores by the melted catalyst. This process renders the exploitation of these catalysts unlikely, unless radically innovative filter concepts are devised.

3.2. Short-distance oxidizing intermediates

3.2.1. Surface oxygen species over perovskites, spinels or other mixed oxides

Investigations by Fino et al. [37] have demonstrated that α-type oxygen chemisorbed on mixed oxides shows remarkable activity under "loose" contact conditions. The amount of active oxygen depends on the number of oxygen vacancies on the oxide surface. Therefore, perovskites, spinels or other mixed oxides that maximize this type of chemisorbed oxygen should be pursued.

3.2.2. Oxygen species over metal-doped CeO_2

Studies by Bueno López et al. [38] have shown that La-doped CeO_2 is characterized by enhanced redox activity and by the presence of surface oxygen species, which, however, can only be spilled over soot to exert their action at short distances, thus requiring a good contact between the catalyst and soot, as well as new catalyst morphologies [19]. In fact, spillover oxygen creates (and regenerates) catalytic sites, which can be used several times [27,39].

4. Soot oxidation kinetics

The kinetics of soot oxidation have been addressed in detail in the literature. One of the first extensive research works on uncatalyzed soot oxidation is that of Neeft et al. [40]: different soot sources were investigated (flame soot-Printex-U and Diesel soot), and the effect of oxygen concentration and the addition of water were described. In particular, it was shown that the reaction order in O_2 is ca. 1, while in soot conversion it is ca. 0.73; the presence of H_2O improves the Printex-U oxidation rate by increasing the associated pre-exponential factor, while the activation energy remains unchanged (168 kJ/mol). The overall similarity between Printex-U and Diesel soot data has suggested the use of Printex-U as a surrogate for Diesel soot laboratory experiments, which is now common practice, as can be seen in the literature. A subsequent work by Yezerets et al. [41] reached similar conclusions by resorting to the step response technique, in order to achieve differential soot consumption in the test and assess the conversion-specific parameters of soot oxidation. The average activation energy was found to be 137 and 132 kJ/mol for Diesel and model soot while the reaction order in O_2 was equal to 0.61 and 0.71, respectively, and almost independent of the temperature.

The effect of NO_2 on soot oxidation is of paramount importance and it is at the basis of Diesel particulate filters operated in passive regeneration mode, which are now known as CRT© (continuously regenerating traps). The higher oxidation potential of NO_2 than O_2 makes it convenient to use the oxidized NO_x from the upstream DOC, which is positioned in a close-coupled position with the trap, in order to oxidize soot at lower temperatures than those that would be obtained if oxygen was used. The oxidation of soot by NO_2 has been described extensively by, among others, Messerer et al. [42] and Tighe et al. [43]. The work of Messerer et al. [42] separately evaluated the contributions of O_2 and NO_2 in the kinetics of soot oxidation, and reached the following conclusions: an activation energy for Diesel soot of around 100 kJ/mol was necessary for O_2-promoted soot combustion, that is, a lower value than reported in earlier studies, and of 40–70 kJ/mol for the NO_2-promoted one. These activation energies can be considered apparent ones, since they include adsorption and reaction contributions, which were calculated by Messerer et al. [42]. Tighe et al. [43] later extended these measurements to different Diesel soot samples with different Diesel qualities (i.e., the nature of the hydrocarbons constituting the Diesel as well as the combustion operating conditions). The resulting activation energies were in the 62 kJ/mol (heavy duty engine) and 72 kJ/mol (ultra-low sulpur Diesel) range for NO_2-promoted soot oxidation.

Zouaoui et al. [44,45] conducted a comprehensive work on uncatalyzed soot oxidation. This work deals with the influence of O_2 and NO_2 on soot oxidation, and provides kinetic parameters for both CO and CO_2 yielding reactions. The cooperative interaction of O_2 and NO_2, which leads to a faster reaction than that which would occur with just an additive contribution of both oxidants, is also pointed out. Moreover, the fostering effect of water which had been already observed experimentally by Neeft et al. [40] is also taken into account. The full set of reactions and associated kinetic expressions is the following (Zouaoui et al. [44]):

$$C + O_2 \rightarrow CO_2 \quad (1)$$

$$C + 0.5O_2 \rightarrow CO \quad (2)$$

$$C + 2NO_2 \rightarrow CO_2 + 2NO \quad (3)$$

$$C + NO_2 \rightarrow CO + NO \quad (4)$$

$$C + NO_2 + 0.5O_2 \rightarrow CO_2 + NO \quad (5)$$

$$C + 0.5O_2(+NO_2) \rightarrow CO(+NO_2) \quad (6)$$

without the water effect:

$$R_{1-6} = \left(k_{1f}X_{O_2} + k_{2f}X_{O_2}\right) + k_{3f}X_{NO_2} + k_{4f}X_{NO_2} + \left(k_{5f} + k_{6f}\right)X_{O_2}^{0.3}X_{N_2O} \quad (7)$$

with the water effect:

$$R_{1-6} = \left(k_{1f}X_{O_2} + k_{2f}X_{O_2}\right)\cdot\left(1 + c(T)X_{H_2O}^{\gamma}\right) + k_{3f}X_{NO_2}\left(1 + a(T)X_{H_2O}^{\alpha}\right) + k_{4f}X_{NO_2}\left(1 + b(T)X_{H_2O}^{\beta}\right) + \left(k_{5f} + k_{16f}\right)X_{O_2}^{0.3}X_{NO_2} \quad (8)$$

where X_i are molar fractions, while k_j are intrinsic kinetic constants expressed as s^{-1} which are intended as grams of soot oxidized per initial gram of soot and per unit time. The activation energy of the O_2 mediated oxidations leading to CO_2 is 127 kJ/mol, while the one that leads to CO is 170 kJ/mol. In a similar way to the NO_2 mediated mechanism, the activation energy are 39 and 66 kJ/mol for CO_2 and CO, respectively. These values are in agreement with the above-mentioned estimations. The full set of pre-exponential values and constants in Eqs. ((1)–(6)) can be found in Zouaoui et al. [44].

However, the CRT© concept requires lower temperatures than those that can be provided by uncatalyzed soot oxidation with NO_2, in order to achieve a real passive regeneration at the Diesel engine outlet temperatures. For this reason, the NO_2 produced by the DOC needs to be re-oxidized several times inside the DPF, in order to

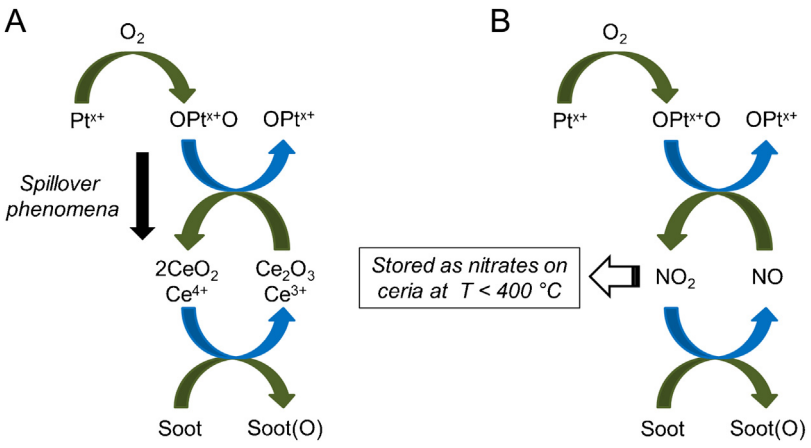

Fig. 1. Redox mechanisms involving CeO_2 and Pt during soot oxidation reaction under O_2 (Section A). Mechanisms taking place on Pt when the same oxidation process is assisted by NO_x (Section B). Adapted from Ref. [47].

use it more than once during its residence time in the filter. This re-oxidation requires a catalyst inside the DPF, that is, namely Platinum, which is very active at such low temperatures (250–350 °C). Jeguirim et al. [45] stated that the individual contributions of O_2 and NO_2 to soot oxidation are only influenced negligibly by Pt, whose main effect is the re-oxidation of NO–NO_2. However, the simultaneous presence of both oxidants has an enhancing effect on soot oxidation, which is fostered by Pt: an overall mechanism involving the formation of atomic oxygen over Pt sites, followed by its transfer to the carbon surface, is established. Thus, the presence of a Pt-based catalyst increases the surface concentration of C(O) complexes, which then react with NO_2, and this leads to enhanced carbon consumption (Jeguirim et al. [45]). Various active supports can be used to load Pt and enhance the soot oxidation activity, e.g., Ceria: the Ce^{4+}/Ce^{3+} redox cycle confers the ability to adsorb gaseous O_2, thus active oxygen is formed at the surface (O_{ads}), which in turn can be transferred to the soot–catalyst interface by superficial diffusion [38,46]. This mechanism coexists with the temporary storage of the adsorbed oxygen as bulk lattice oxygen, which is then delivered as active O_{ads} to the catalyst surface. The redox processes that take place during the catalyzed oxidation of soot, either in the presence or absence of NO_x, are schematized in Fig. 1. The buffering properties of Ceria with Pt allow the dissociated O formed on Pt through spillover phenomena to be conferred at the soot–catalyst contact points (Section A) [47]. In the co-presence of O_2 and NO_2, Ceria also acts as a storage mean of NO_2 under the form of nitrate at low-to-moderate temperatures (below 400 °C). Above these temperatures, NO–NO_2 oxidation would very limited due to thermodynamic equilibrium, while the stored NO_2 can be released from the Ceria to the soot oxidation reaction (Section B) [47].

4.1. Catalytic soot oxidation over Ceria-based catalysts: kinetics and reaction mechanisms

Over the years, many works have considered the reaction mechanisms of soot combustion for non catalytic [41,42,48–50] or catalytic processes [51–59]. However, detailed kinetic studies have not been reported in most of these publications. A reason for the lack of good kinetic models is that this catalytic system is highly complex, involving two solid phases (catalyst and soot) and a gas phase (oxygen and reaction products such as carbon dioxide). These three phases have to be in close contact to make it possible the reaction and then the intensity of physical interaction between the soot and the catalyst determines the reaction rate. Therefore, an accurate description of soot combustion over solid catalysts requires a multi-population kinetics approach [60]. Ceria is one of the most effective materials for soot combustion, due to its excellent oxygen-buffering capacity, and hence many studies have been dedicated to the kinetic and reaction mechanism of soot with CeO_2 as redox catalyst. Based on the experimental evidence, Gross et al. [61] proposed a reaction mechanism for the catalytic combustion of soot on Ceria involving the formation of superoxides, peroxides, oxygen vacancies, surface diffusion and the change of type of contact between the carbon and the catalyst during the combustion. The reaction mechanism is rather complex and several steps are involved:

$$n\mathrm{CeO}_x + \mathrm{O}_2 \rightarrow [n\mathrm{CeO}_x]^{+}\mathrm{O}_2^{-} \quad (9)$$

(formation of superoxide species)

$$[n\mathrm{CeO}_x]^{+}\mathrm{O}_2^{-} \leftrightarrow [n\mathrm{CeO}_x]^{2+}\mathrm{O}_2^{2-} \quad (10)$$

(conversion of superoxide into peroxide ions)

$$[n\mathrm{CeO}_x]^{+}\mathrm{O}_2^{-} \leftrightarrow n\mathrm{CeO}_y \quad (11)$$

(conversion of superoxide into the oxidized form of cerium oxide, 'y' being greater than 'x')

$$[n\mathrm{CeO}_x]^{2+}\mathrm{O}_2^{2-} + \mathrm{C} \rightarrow [n\mathrm{CeO}_x]^{2+}[\mathrm{CO}_2]^{2-} \quad (12)$$

$$[n\mathrm{CeO}_x]^{2+}[\mathrm{CO}_2]^{2-} \rightarrow [n\mathrm{CeO}_x]^{2+}[]^{2-} + \mathrm{CO}_2 \quad (13)$$

(reaction of peroxide with soot and formation of carbon dioxide)

$$[n\mathrm{CeO}_x]^{2+}[]^{2-} \rightarrow n\mathrm{CeO}_x \quad (14)$$

(diffusion of oxygen species to yield reduced sites).

This is a strict mechanism, however, according to both experimental and theoretical evidences, some simplifications can be actuated in the kinetic model considering the relative rates of each step [62]. Then, the following simplifications have been actuated: (i) peroxides ions do not form superoxides ions; this means that peroxides are the active oxygen species that react with soot and it is supposed that this reaction is faster than the reaction that yields superoxides; (ii) the steps that describe CO desorption and the oxygen vacancy migration are fast; (iii) not all the carbon atoms of soot are in contact with the catalyst; then, it has to be considered the combustion of carbon atoms that are not in the interface catalyst–soot (namely, C*). During the reaction, those carbon atoms that initially were not in contact with the catalyst, may change their position from the soot–gas interface to the soot–catalyst interface (C* → C). This dynamic behavior is not only due to the movement of the carbon, but also to the movement of the active species on the catalyst surface. The carbon atoms that are in the catalyst-soot interface are reached by oxygen surface diffusion, whereas those that are in the soot-gas interface are reached by oxygen spillover.

Moreover, it must be pointed out that the calcination conditions of Ceria has an important effect on the catalytic activity: as the calcination temperature increases (i.e., from 450 to 800 °C), the amount of cerium superoxide and peroxide increases, thus accelerating the combustion reaction.

The equations to be considered to model the kinetics of soot combustion, taking into account the reaction steps of the proposed mechanism, are the following:

$$\frac{\partial[n\mathrm{CeO}_x]}{\partial t} = -k_1 \cdot [\mathrm{CeO}_x] \cdot P_{\mathrm{O}_2} + k_2 \cdot \left[[\mathrm{CeO}_x]^{2+}\mathrm{O}_2^{2-}\right] \cdot [\mathrm{C}] + k_3 \cdot \left[[\mathrm{CeO}_x]^{2+}\mathrm{O}_2^{2-}\right] \cdot [\mathrm{C}^*] \quad (15)$$

$$\frac{\partial\left[[n\mathrm{CeO}_x]^{+}\mathrm{O}_2^{-}\right]}{\partial t} = k_1 \cdot [\mathrm{CeO}_x] \cdot P_{\mathrm{O}_2} - k_4 \cdot \left[[\mathrm{CeO}_x]^{+}\mathrm{O}_2^{-}\right] \quad (16)$$

$$\partial[[n\mathrm{CeO}_x]^{2+}\mathrm{O}_2{}^{2-}]/\partial t = k_4 \cdot [[\mathrm{CeO}_x]^{+}\mathrm{O}_2{}^{-}] - k_2 \cdot [[\mathrm{CeO}_x]^{2+}\mathrm{O}_2{}^{2-}] \cdot [\mathrm{C}] - k_3 \cdot [[\mathrm{CeO}_x]^{2+}\mathrm{O}_2{}^{2-}] \cdot [\mathrm{C}^*] \quad (17)$$

$$\partial[\mathrm{C}]/\partial t = -k_2 \cdot [[\mathrm{CeO}_x]^{2+}\mathrm{O}_2{}^{2-}] \cdot [\mathrm{C}] + k_5 \cdot [\mathrm{C}^*] \quad (18)$$

$$\partial[\mathrm{C}^*]/\partial t = -k_3 \cdot [[\mathrm{CeO}_x]^{2+}\mathrm{O}_2{}^{2-}] \cdot [\mathrm{C}^*] - k_5 \cdot [\mathrm{C}^*] \quad (19)$$

$$F_{\mathrm{CO}_2} = W_c \cdot \left\{k_2 \left[[\mathrm{CeO}_x]^{2+}\mathrm{O}_2^{2-}\right] \cdot [\mathrm{C}] + k_3 \cdot \left[[\mathrm{CeO}_x]^{2+}\mathrm{O}_2^{2-}\right] \cdot [\mathrm{C}^*]\right\} \quad (20)$$

In which k_i represent the kinetic rate constants of the reaction steps in the above described mechanism. The concentration of each species in the set of equations is given in mol/g, w_c (g) is the mass of catalyst, and F_{CO_2} (mol s^{-1}) the molar flow of CO_2 at the reactor exit. This reaction mechanism is valid for a tight-contact mode between the soot and the catalyst. In order to simulate the operating conditions of a real catalytic trap, the mechanism has to be coupled with mass and energy transfer steps. Nevertheless, it is difficult to develop such complete model of this catalytic system. Another approach could be to evaluate global kinetic parameters that can fit the kinetic response of the catalytic system under loose-contact mode. The latter case corresponds to an empirical model that might be useful for design purposes, but will not provide a detailed description of the reaction mechanism [62].

5. Classification of soot oxidation catalysts

Many soot oxidation catalysts have been studied since the early 1980s, as soot combustion is a total oxidation reaction and hence sophisticated materials, with appropriate physico-chemical proprieties, are not required [3,6–19]. Although noble metal-based catalysts have dominated the automotive exhaust catalysis area, mainly because of their high catalytic activity and stability, their limited availability and high costs have always been a reason for the search for alternative catalysts [63]. A number of non-noble metal materials have been found to be active for the oxidation of soot in catalyzed Diesel filters [64,65]. The most recent synthesis procedures focus on stable materials that exhibit good mobility of the oxidizing species and, if possible, they should be active on NO_x abatement (vide supra). The latter systems include different mobile catalysts:

(i) *Ceria-based catalysts,* which have received a great deal of attention because CeO_2 alone, or in combination with other metals/metal oxides, may exhibit promising soot oxidation activity [1–3,6–25,64–66]. Thus, zirconium and many rare earth elements (e.g., La, Pr, Sm, Y, Gd, Tb, Lu, Hf and Nd) have been introduced into the Ceria framework to improve the oxidation activity (=oxygen storage capacity and redox properties) of CeO_2-based materials and their stability at high temperatures. The redox behavior and the availability of chemisorbed oxygen (α-species) are important factors in the oxidation activity of Ceria based materials [67–69]. Bueno López et al. [38] have provided evidence of the involvement of CeO_2 lattice oxygen in soot oxidation (via a Mars–van Krevelen mechanism [1,3,19]), although details on the reaction mechanisms have yet to be clarified [19].

Over the years, there has been significant progress in the nanoscale controlled synthesis of CeO_2-based materials for catalysis. Many Ceria nanostructures have been synthesized using methods designed by various research groups (e.g., Piumetti et al. [21] prepared CeO_2-nanocubes of ca. 50–150 nm, which have been shown to be very effective for soot combustion, Fig. 2). Ceria nanomaterials with well-defined reactive (1 0 0) and (1 1 0) planes are usually more active than conventional polycrystalline Ceria NPs with preferred exposure of (1 1 1) planes [21]. Data reported for several catalytic reactions suggest that the order of chemical reactivity for CeO_2-nanostructures is nanocubes > nanofibers > polycrystalline Ceria NPs [21]. This sequence reflects the reverse order of the surface stability of Ceria: (1 0 0) and (1 1 0) < (1 1 1) facets. However, the beneficial role of the textural properties (e.g., specific surface area, total pore volume, pore diameter and so on) on the overall catalytic activity of CeO_2 for various reactions, including soot combustion, is well known. Therefore, it is necessary to maximize the exposure of more reactive surfaces of CeO_2 using high surface area materials as supports, to be coated on the filter wall surface.

On the other hand, nanofibers are mainly characterized by (1 1 1) facets [25] and low specific surface areas (SSA) [13,25] and are in principle less reactive towards soot oxidation than highly porous materials, especially in terms of onset temperature. However, thanks to the nanofibers' ability to form randomly arranged networks, which increase the number of soot-fiber contact points by allowing a better penetration of soot in the nanofiber structure, the soot oxidation activity can be enhanced under specific conditions of loose contact [13]. The coated layers of nanofibers on DPF walls possess a high open porosity, and thus a low associated pressure drop, and may lead to overall lower oxidation temperatures with respect to polycrystalline Ceria NPs, provided that their structure is fully retained in the coating process [25].

Guillén-Hurtado et al. [70] have synthesized a new $Ce_{0.5}Pr_{0.5}O_2$ mixed oxide, with high surface area (125 $m^2\,g^{-1}$) and small particle size (7 nm). The latter catalyst has been tested under NO_x-containing gas mixtures, and has proven to be even more active than a Pt-based commercial catalyst. Nanostructured materials are interesting because of their small-featured size, which endows them with size- and shape-dependent properties due to the high surface-to-volume ratio (a higher number of coordinatively unsaturated sites), and their unique electronic features (quantum size effects) [71–75]. The higher activity of nanostructured Ceria-based materials has been confirmed in several reactions, such as CO oxidation, the CO_2 reforming of methane, methanol and ethanol reforming, low-temperature WGS and, more recently, soot oxidation [21,76–79].

Wei et al. [80] have successfully synthesized three-dimensionally ordered macroporous (3DOM) $Au/Ce_{1-x}Zr_xO_2$, $Au\text{-}CeO_2/ZrO_2$ and $Au\text{-}Pt/Ce_{1-x}Zr_xO_2$ catalysts; they found that with the assistance of NO_x, these catalysts could decrease the ignition temperature of soot to lower than 250 °C, even in loose contact conditions. In absence of NO_x, the advantages of Pt should

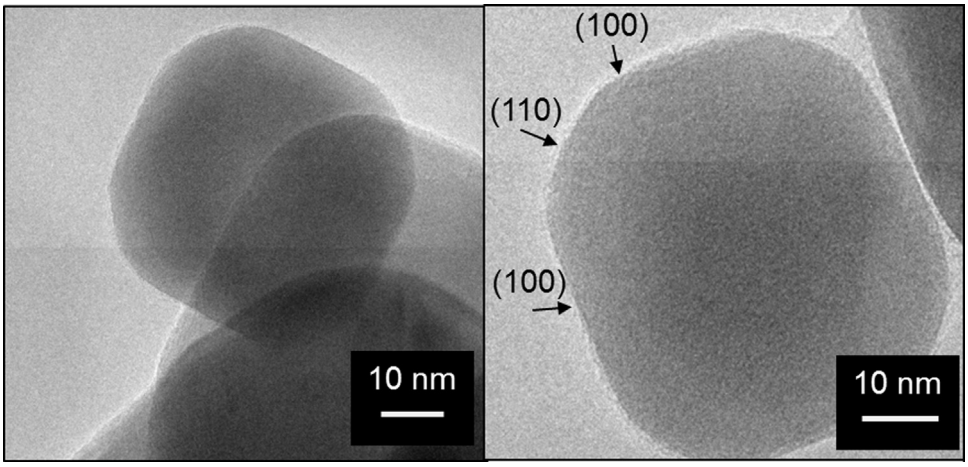

Fig. 2. TEM images of CeO_2 nanocubes effective for soot oxidation reaction. Adapted from Ref. [21].

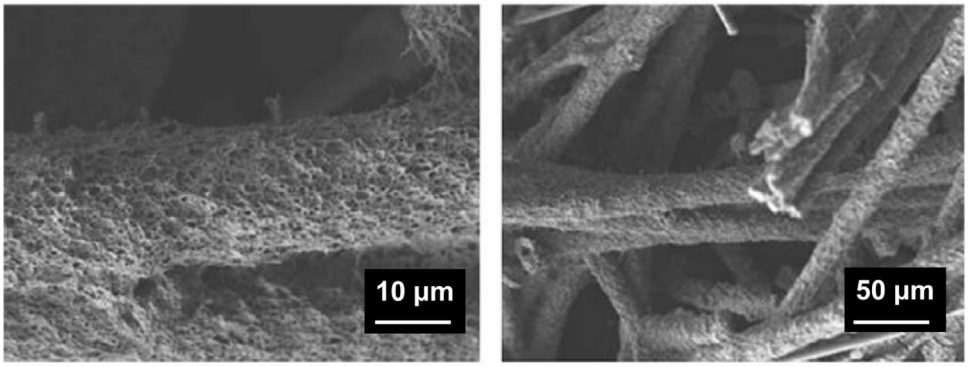

Fig. 3. SEM images of a nanofibrous $LaMnO_3$ catalyst on silica fibers. Adapted from Ref. [94].

be markedly weakened [81]. Indeed, Ceria–zirconia nanocatalysts (either porous or non-porous systems) are active for soot combustion [82].

(ii) *Perovskite/spinel/hydrotalcite/delafossite catalysts* which have received attention because they are rather stable materials [83,84] that are able to deliver oxidizing species and promote NO_x decomposition [85]. The main findings in this area are:

- General Motors (GM) researchers have claimed that Sr-doped $LaMnO_3$ materials have been employed successfully to substitute Pt in both DOC (Diesel Oxidation Catalysts) and in NSC (NO_x Storage Catalysts), thereby paving the way towards less expensive catalysts [86].
- Li et al. [87,88]; Ura et al. [89] have shown that K-promoted CoMgAlO hydrotalcite can not only favor soot combustion, but can also lead to a 30% conversion of NO_x under "real" conditions.
- Lin et al. [90] have shown surprisingly high activity of $BaAl_2O_4$ systems for the simultaneous combustion of soot and the removal of NO_x, even under "loose" contact conditions.
- Apart from the Authors' work on Li- and Ni-based perovskites, which guarantee high α-oxygen availability (Fino et al. [91]), other researchers have studied perovskite catalysts for soot combustion purposes. The developments that deal with metals that are suitable for exploitation in an aftertreatment system (e.g., La-Sr FeO_3 perovskites [92]; La-K-$CoFeO_3$ [93]; nanofibrous $LaMnO_3$ catalysts [94]) are particularly interesting. Lanthanum ferrites have also been shown (Furfori et al. [95,96]) to act as catalysts in the reduction of NO_x with in-situ generation of H_2 using a small on-board reformer. The same property has also been exhibited in mixed oxide catalysts, such as $Ce_2Zr_{1.5}Me_{0.5}O_8$ (with Me = Co, Rh, or Co-Noble Metal [97]). Nanofibre materials could be suitable for the tailoring of new catalytic layers, thus offering the possibility of closer contact between the catalyst and soot. Fig. 3 shows SEM images of fibrous-oxide $LaMnO_3$ catalysts obtained on silica fibers [94]. The silica fibers were coated with a 6-μm-thick layer of nanofibrous $LaMnO_3$ and the final diameter of the rods was about 20 μm. The latter catalysts have resulted to be highly effective soot trapping and combustion systems [94].
- Lithium Chromite delafossites were investigated by the Authors from powder catalysts to the full-scale filter, obtaining the best performances with the Cr sub-stoichiometric formulation ($LiCr_{0.9}O_2$) [98]. The so-catalyzed trap reached a one-third fold reduction of the time required for the filter regeneration (and of the related fuel penalty) as well as a much more complete regeneration compared to that of a non-catalytic trap.

(iii) Other metal oxides/mixed metal oxides, which are possibly even more stable than the above-mentioned counterparts and rather easy to be synthesized.The following results have been obtained in recent years:

- Sánchez et al. [99] have shown that La_2O_3 doped with K, Rh or Pt can promote a simultaneous reduction of NO_x and soot, although only under "tight" contact conditions.
- Castoldi et al. [31] have shown that alkaline and alkaline-earth metal oxides, under "loose" contact conditions, exhibit catalytic activity that is proportional to the electronegativity of the contained metal (vide supra).

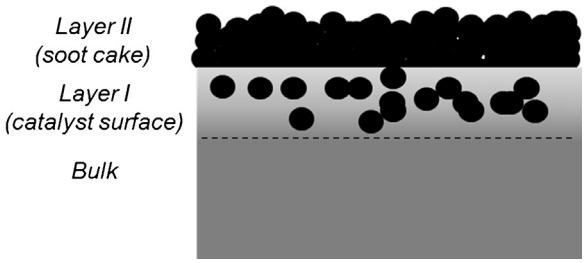

Fig. 4. Scheme of the DPF wall, catalytic-coating-influenced Layer I and top Layer II which is not in the sphere of influence of the catalyst. Adapted from Ref. [102].

- Olong et al. [100] in an extensive study commissioned by Bosch, pointed out that exceptional soot oxidation activity is obtained with $Pb_{10}La_5Co_{85}O_x$ catalyst, although they expressed some doubts regarding the applicability of Pb. Moreover, these Authors showed that Cs_3Co_{97} oxides are promising soot oxidation catalysts, with better stability than K-promoted Ceria catalysts.
- Recently, a hierarchically porous zeolite beta has been prepared via surfactant-assisted hydrothermal treatment and subsequent alkali etching approach [101]. High Cu and Mn contents were then dispersed into the as-synthesized hierarchically porous zeolite beta. The composite catalyst exhibited high activity and stability for soot oxidation, mainly due to a synergetic effect between valence-varied active species Cu^{n+} and Mn^{n+}. In addition, the obtained catalyst revealed excellent water resistance, as a consequence of the hydrophobic crystalline zeolite framework.

In order to meet future expectations favoring Diesel engines, it is necessary to develop catalysts with high performances and robustness but low costs. Therefore, efforts should be addressed towards the development of solid catalysts that decrease, or eliminate, the use of Pt and other precious metals.

In particular, CeO_2-nanostructures [21] have shown a good thermal stability during multiple TPO tests (e.g., up to 700 °C for a couple of hours in the absence of steam), although accelerated deactivation tests (e.g., 50 h at 850 °C in 10% steam) are necessary to evaluate possible candidates for real application in DPFs.

6. Study of the soot–catalyst interaction phenomena

6.1. Modelling

On the grounds of experimental evidence, a "Two-Layer model" has often been used to account for the 2-stage reaction rate pattern of soot combustion during TPO runs. This model was first developed by Lorentzou et al. [102] to describe the influence of soot–catalyst proximity, as schematized in Fig. 4. In can be observed that "Layer I" is a region over which a spatial "field of catalyst activity" exists. Soot particles oxidize when they are within this region and are in contact with the catalyst surface. This layer can "load" an appropriate amount of soot (which depends on the coating structure and filtration velocity) until it is filled. "Layer II" (or the soot cake layer) is instead formed by soot particles that form a "queue" on top of the filled catalyst Layer I. The model considers an exchange of soot between the two zones, according to the following equations:

$$-d\frac{y_1}{dt} = k_y y_1^{2/3} \frac{m_{cat}}{m_{01}} P_{O_2}^{1/2} \quad (21)$$

$$-d\frac{y_2}{dt} = k_y (1-y_1)^n y_2^{2/3} \frac{m_{cat}}{m_{01}} P_{O_2}^{1/2} \quad (22)$$

$$m_{01} + m_{02} = m_0 \quad (23)$$

where y_1 and y_2 are, respectively, the ratios of the current masses (m_1 and m_2) to the initial masses (m_{01} and m_{02}) of soot pertaining to the first and the second fractions, which are implicitly contained in the model as parameters.

As a whole, the soot combustion rate in catalyzed filters exhibits two-peaks (bi-modal distribution) versus temperature. Experiments have been carried out heating the filter at a fixed rate (3 °C/min) under 10% O_2 in N_2. The lower temperature peak mainly originates from the catalytic oxidation of soot, while the second peak at a higher temperature, appears as a consequence of the thermally oxidized soot. The Two-Layer model is able to describe the soot oxidation rates of different catalyzed filters with an accuracy of ±5% [102]. Similar approaches have also been proposed by the Authors' research group and by Ciambelli for TPC runs on catalyst-soot powder mixtures, to justify the presence of two combustion modes [103]. However, the weak feature of this approach is that it is not an "a-priori method" and any fitting parameter can account for other phenomena beyond contact. Some early speculations made by the Authors' group [35] were in fair agreement. It has been shown, on the grounds of an Ozawa kinetics analysis of DSC catalyzed soot combustion conducted through a kinetics assessment, that soot combustion on Cu–K–V–Cl catalysts does not only depend on the soot–catalyst interaction, but also on the morphology of the soot particles. Therefore, further studies have to be conducted to take into account the morphology of soot particles in the model. Soot reactivity (in terms of soot oxidation temperature) was correlated to the crystallinity of soot by using TEM [104], although not fully quantitatively. Low-aromatic fuels showed more crystallite structures, clear union spheres, and more ordered morphology than high-aromatic fuels. Conversely, the highly ordered, crystalline structure requires much more energy to be oxidized than for the less ordered structure (the latter especially at the defect points in the structure). As a result, model soot, namely Printex-U, could even be less refractory to oxidation than the soot originated from recent fuels, which are characterized by a poor aromatic content [104].

6.2. In-situ microscopy characterization

The pioneers in this area are the "Industrial Catalysis" researchers at Delft University who, together with the "reactor and catalysis engineering" group of Delft University of Technology [105,106] first tested the occurrence of catalyzed soot combustion in an in-situ reactor placed in a Raman spectrometer. The same research group then moved onto visible microscopy [36], and the researchers were able to take in-situ micrographies, like those reported in Fig. 5, related to $Cs_2SO_2{\cdot}V_2O_5$ catalyst–soot mixtures. Among the most interesting findings of these researchers, the following are worth mentioning:

- the $CsSO_4{\cdot}V_2O_5$ catalyst actually "moves" and does so even before melting;
- when the catalyst is molten, it becomes very active and the reaction rate is maximized;
- the observation, coupled with image processing, can be used to estimate soot combustion kinetics, even though some pitfalls of this procedure (mostly related to 2-D imaging) have been pointed out by the researchers.

These visible microscopy studies have revealed the possible presence of moving sites and possible molten salts that catalyze soot oxidation, thus confirming the dynamic behavior of a soot combustion reaction over solid catalysts.

Similar tests have also been performed by Fino et al. [34] in a heated microscope: the pictures reported in Fig. 6 show that, at 360 °C, the $Cs_2O{\cdot}V_2O_5$ catalyst droplet does not tend to "wet" the carbon tablet on which it is located, and the contact between the catalyst and carbon remains limited (solid catalyst). However, at

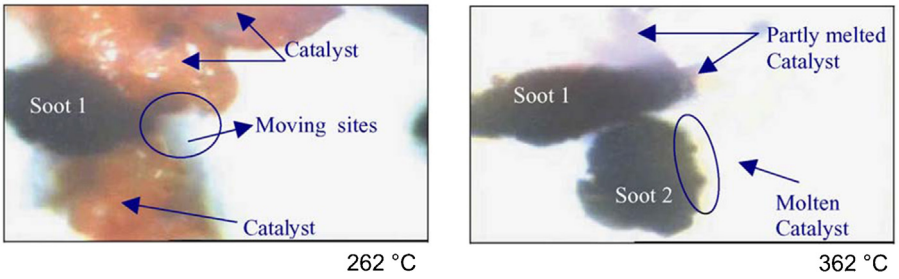

Fig. 5. Microscope images of a $Cs_2SO_2{\cdot}V_2O_5$ catalyst-soot mixture, taken at 262 °C and 362 °C. Soot 1 and 2 represent two different soot particles. The images were taken at a magnification of 50×. Adapted from Ref. [106].

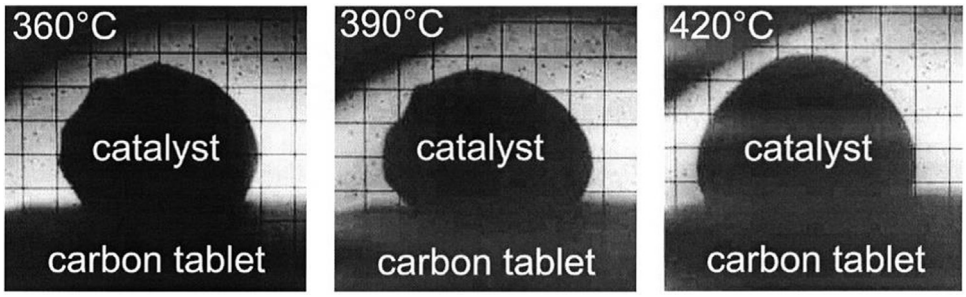

Fig. 6. Images of a $Cs_2O{\cdot}V_2O_5$ sample obtained in a thermal microscope under calm air: (a) 360 °C (solid catalyst); (b) 390 °C (slightly before the start of eutectic liquid formation); (c) 420 °C (molten catalyst). From Ref. [34].

higher temperatures (namely at 390 and 420 °C), a better interaction between the carbon and catalyst particle can be observed, due to the partially melted catalyst.

It is important to consider the oxidation process as it actually occurs, in a real catalyzed filter. In this context, a detailed analysis has been carried out by Yapaulo et al. [107] on the fate of soot in real DPF filters, with special attention being paid to the intra-wall distribution: VP-SEM images of wafer samples loaded onto a barely soot cake were obtained at two filtration velocities (4 and 8 cm/s) in order to reveal the soot penetration depth and distribution within the wall of the wafers and how these are affected by different filtration conditions. Carbon maps, collected at different locations along the cross-section of the wafers loaded with soot were obtained. From the data obtained by Yapaulo et al. [107] it can be stated that:

- The filtration velocity has a significant effect on the wall loading performance of the filter. It changes the partitioning between the soot trapped in the wall and on the filter surface (soot cake layer). In fact, filling wafers with a higher filtration velocity resulted in a higher wall loading capacity.
- The filtration velocity does not affect the soot penetration depth in the filter wall. These data, along with the observed higher wall loading capacity with a higher filtration velocity, imply that the soot has a higher packing density within the wall as a direct result of the higher filtration velocity.
- The characteristics of the soot significantly affect both wall loading and soot cake layer performance. The slope of the pressure drop curve during soot cake layer growth is more dependent on soot characteristics than on the filtration velocity. I fact, wall loading is more limited when the wafer is filled by smaller particles in a lower concentration exhaust flow.
- Imaging results from the VP-SEM analysis suggest that loading the wafers with smaller particles results in a deeper soot penetration in the wall. This means that the soot penetration depth is governed more by the particulate characteristics than by the filtration velocity.
- Imaging results from all the loading cases suggest that, although some soot manages to penetrate deep into the wall, the majority of the soot stays very close to the wall surface.

Similar investigations need to be carried out on catalytically wash-coated filters, and it is also necessary to obtain new insights into this research area via the use of non-destructive analyses e.g., micro-nanotomography or visible microscopy analyses in newly conceived rigs. An interesting approach introduced to non-destructively measure CeO_2-Carbon black (CB) systems has been shown by Issa et al. [108], who found that whenever CeO_2 and CB are in close contact, a new signal can be recorded by means of Electron Paramagnetic Resonance (EPR). This technique paves the way towards rapid and effective contact assessment methods under real operating conditions: hence, a more recent work exploiting this technique is the one of Toops et al. [109], who measured the soot cake profiles during normal filtration mode as well as during regeneration along time, thus achieving to assess experimentally the local soot cake density.

6.3. Contact conditions between soot and catalyst

The particle number and size distribution are important aspects to qualify Diesel engine emissions, considering the new limits, in term of particle number, of Euro 6 regulations. In this scenario it is important to study particulate matter (PM) emissions, not only during engine normal operating mode, but also during Diesel particulate filter (DPF) regeneration processes. The results have shown that, under normal operating conditions, the engine and DOC outlet particle number and mass size distributions appear to be very similar, with a peak diameter around 60 nm, while the DPF exhibits high values of filtration efficiency on a particle number basis, even in the nanoparticle range (Fig. 7). Regeneration mode causes a particle number increase of one order of magnitude, with a substantial shift of the number distribution peaks toward larger diameters (it shifts from 60 nm to 150 nm during regeneration) [110]. These are all gas-phase concentrations. Once soot deposits inside the filter, it

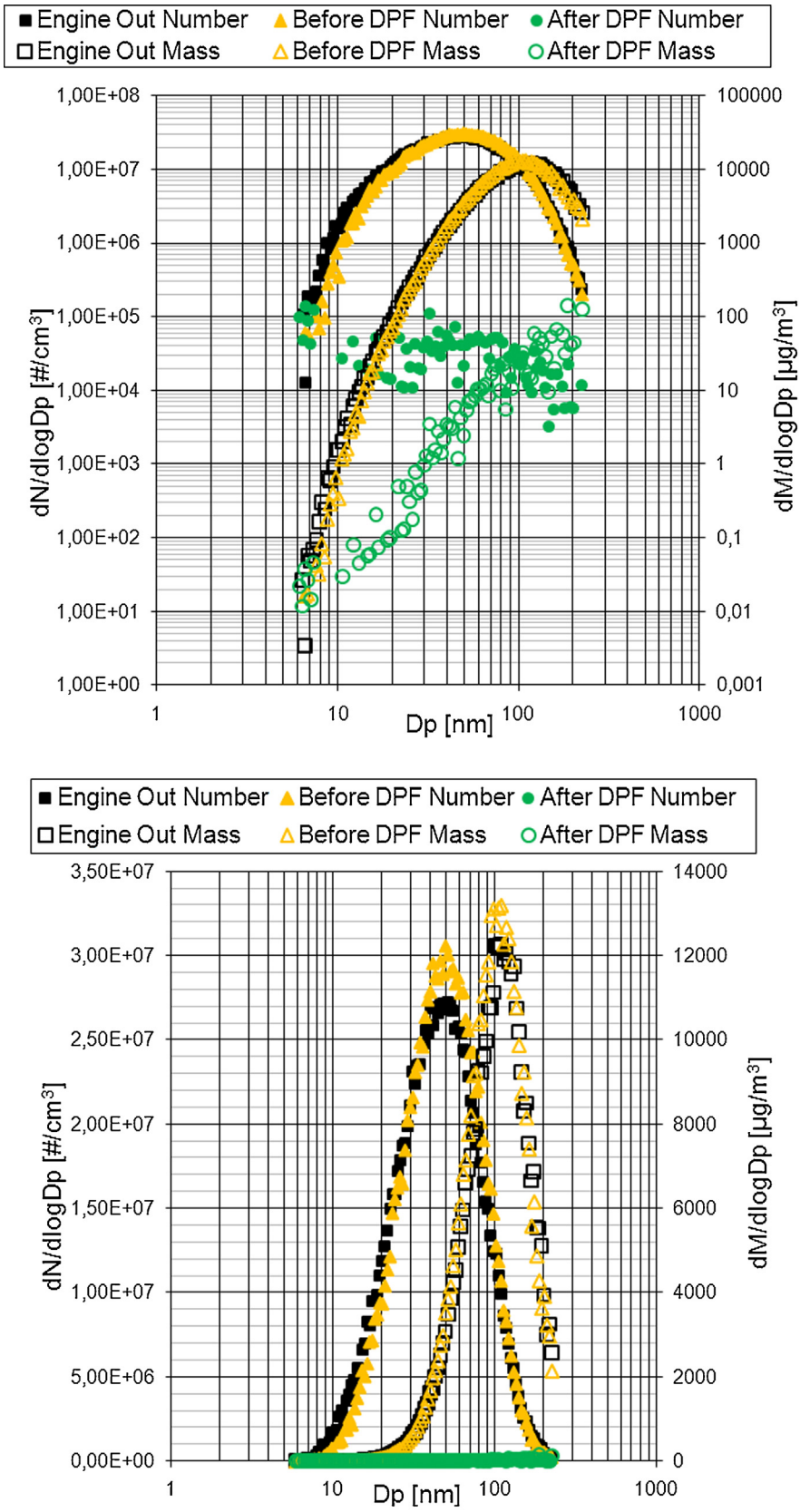

Fig. 7. Particle number (left *y* axis) and mass (right *y* axis) size distributions, emitted by a light duty Diesel engine (4 stokes, 1248 cm^3, 4 cylinders in line, maximum power of 55 kW @ 4000 rpm, bore × stroke: 69.6 mm × 82 mm, compression ratio of 16.8:1) at 1750 rpm/3.5 bar bmep. Log (top) and linear (bottom) *y* axis scales. Adapted from Ref. [110].

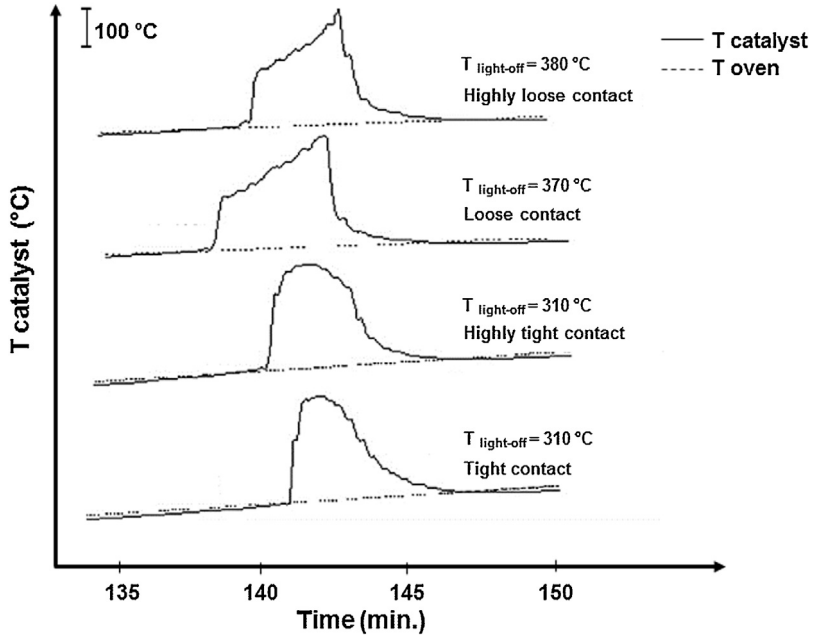

Fig. 8. Light-off for soot combustion as a function of the contact type between the catalyst and the soot: 40 mg soot/400 mg CeO_2 under 40 mL/min 50% O_2/Ar. Adapted from Ref. [111].

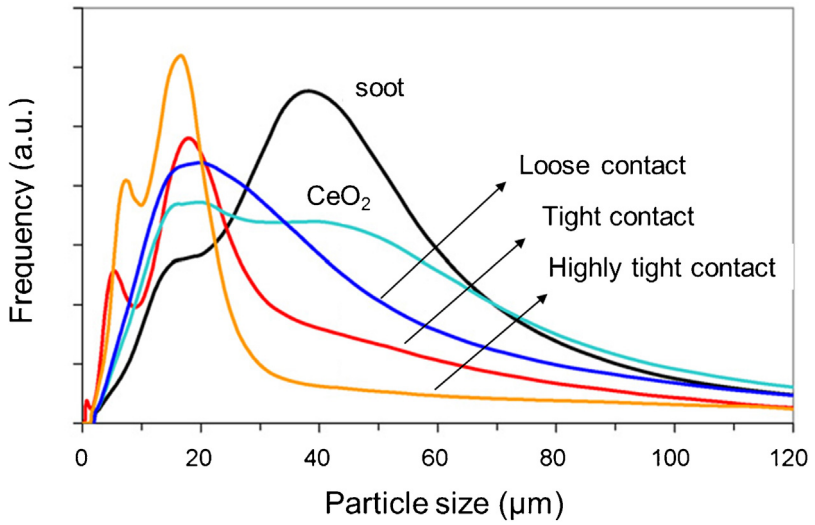

Fig. 9. Particle size distribution of soot, Ceria and soot–Ceria mixtures in "loose", "tight" and "highly tight" contact conditions. Adapted from Ref. [111].

forms a cake in which the original particle size and morphology is not retained, since pressure exerts a force that compacts the soot layer. This new "agglomerate" at the micrometer scale is directly in contact with the catalytic layer underneath, which is coated on the filter wall surface. The contact degree between the catalyst and the cake is of paramount importance in the estimation of soot oxidation kinetics.

In this regard, Iojoiu et al. [111] have conducted a study on the reaction mixtures of soot and Ceria catalysts, prepared according to four different procedures: (i) shaking the two powders directly in the reactor ("highly loose contact"); (ii) mixing soot and the catalyst with a spatula ("loose contact"); (iii) grinding Ceria and soot in a mortar ("tight contact"); (iv) ball milling of Ceria and soot ("highly tight contact"). The soot sample was collected from Diesel engine exhausts through filtration. The catalytic activities obtained as a function of time (Fig. 8) did not show any significant difference between the two "loose" contact conditions and the "tight" ones. However, the light-off temperature in the "loose" condition is 60 °C higher than that of "tight" contact. Moreover, for "tight" contact conditions, the temperature increases very rapidly after soot ignition and reaches a maximum peak in a short time (few seconds), as does the CO_2 signal. Conversely, in the case of "loose" contact conditions, the temperature increases slowly and reaches the light-off temperature for the thermal combustion of the soot at 370 °C, which then takes place more progressively. Moreover, the particle size distributions of the Ceria catalyst and soot in the mixtures have been studied for "loose", "tight" and "highly tight" contact conditions. It has been observed that, despite applying quite strong mechanical forces to the soot-catalyst mixture, it is not possible to break the soot-catalyst aggregates down to less than a few microns, thus showing a bi-modal distribution of the particle sizes, with the main peak centered at about 15 μm (Fig. 9) [111].

Using a Raman-probe microscope, the same Authors noticed that "loose" contact states are characterized by the presence of soot

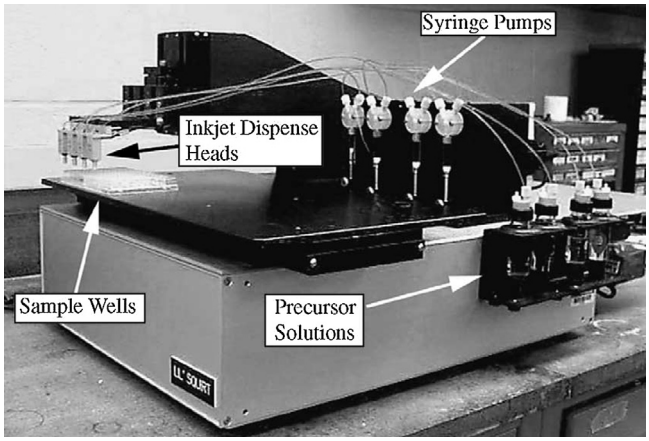

Fig. 10. Inkjet dispensing system used for library synthesis. From Ref. [113].

rich and Ceria rich zones. Whenever soot is taken from powder, van der Waals forces give rise to larger agglomerates (up to 500 μm) than the original soot particles in the exhaust line [110,112]. Consequently, there is still need to study soot-catalyst contact dynamics more realistically by loading real soot onto catalytic filters under operating conditions.

7. Combinatorial catalysis

Over the last few years, there has been some interest in fast screening catalyst compositions for many catalytic reactions, including soot combustion. Among the various attempts, two major works are worth mentioning:

- The work by Reichenbach et al. [113], which can be considered pioneering. Their approach was based on the use of a library of catalysts prepared on a support plate by means of a so-called polymerizable-complex-method from organic precursor solutions dispensed along with metal nitrate solutions. Fig. 10 shows the drop-on-demand printer that was used to prepare the soot oxidation catalysts; the latter combines syringe pumps with inkjet dispensers and incorporates a computer controlled *x–y–z* table. This device allows binary libraries to be obtained with 15 elements generated using precursor solutions. After deposition, each library can be processed to synthesize the final oxide powders [113]. Then, soot-catalysts mixtures can be prepared either manually (the soot solution is usually dispensed using a pipette) or through the ink-jet dispersing apparatus under suspension of a solvent, which evaporates quickly. The final sample is then heated in the combinatorial library sample holder and the soot combustion effect of each catalyst spot is revealed by means of an infrared (IR) camera, as schematized in Fig. 11. This technique was used to characterize the soot oxidation with Ce–K–O, Cu–K–O, Ce–Na–O and Cu–Na–O systems. The conclusion of this study was that both K and Na are very effective in reducing the onset temperature of soot oxidation temperature, as compared CuO or CeO_2 alone. However, some problems can emerge when this technique is used:
  i) the powder caps may collapse when the soot is dosed.
  ii) the behavior changes from cap to cap, and an uneven picture can therefore be taken by the camera, thus causing problems as far as the reliability of the method is concerned;
  iii) radiant effects from the walls may disturb the measurements;
  iv) the soot layer covering the samples may shade the thermal effect;
  v) the thermal effects can be too small to be revealed by the IR camera.

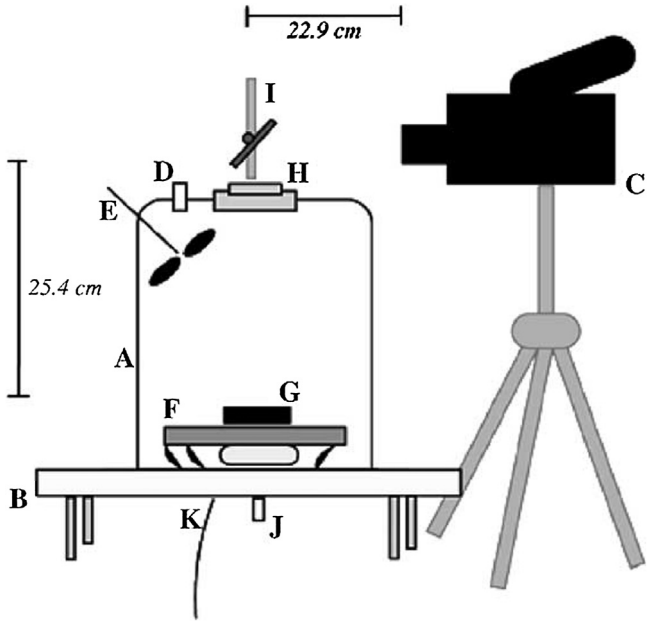

Fig. 11. Scheme of the infrared (IR) catalyst characterization system: (A) outer aluminium reactor wall; (B) base plate; (C) prism DS IR camera; (D) gas inlet; (E) fan; (F) thermofoil heater; (G) combinatorial library sample holder; (H) CaF_2 window; (I) mirror and stand; (J) gas exhaust port; (K) thermocouple and furnace power leads. From Ref. [113].

- Olong et al. [100] tackled some of the above problems with a screening technique using "emissivity-corrected IR thermography" that was capable of perceiving temperature differences of 0.02°. They studied "loose" contact mixtures of soot and catalysts and dosed them in parallel reaction wells on a plate placed inside the IR vision apparatus (Fig. 12). An IR transparent window on the top of the reactor allowed the temperature changes to be recorded directly by the IR-Camera at the desired reaction conditions (e.g., flow rate/composition, TOS, temperature, etc.). An example of these primary catalyst screening data is shown in Fig. 13: at the reaction temperature of 350 °C (Section A), only the $Pb_{10}La_5Co_{85}$ catalyst is considerably active; when the catalyst library is tested at 400 °C (Section B), another two catalysts (namely $Na_{10}La_5Co_{85}$ and $Ce_{10}La_5Co_{85}$) become active and the activity of $Pb_{10}La_5Co_{85}$ decreases since most of the soot has already been combusted at a lower temperature.

8. Highlights on the development of multifunctional traps: modelling approaches

DPFs are highly complex chemical reactors that combine multiphase reactions, separation and material transformations over a range of temporal and spatial domains [2,3,16]. The huge potential market impact, as well as the spin-off potential to many other fields (e.g., TPOX, laser printers, etc.), justify a concerted effort to improve the current level of understanding of these multifunctional catalytic systems.

An interesting arena for the modelling and simulation of DPFs has been shown by Konstandopoulos et al. [17]. The multiscale nature of DPFs can be reflected through various orders of magnitude, as schematized in Fig. 14. Such scales have often been addressed through modelling approaches, though very rarely connected to one another, mainly because of computational difficulties. When parts of a system are independent, they do not provide redundant information and cannot be visible at a large-scale. Independence indicates a large quantity of information at a fine

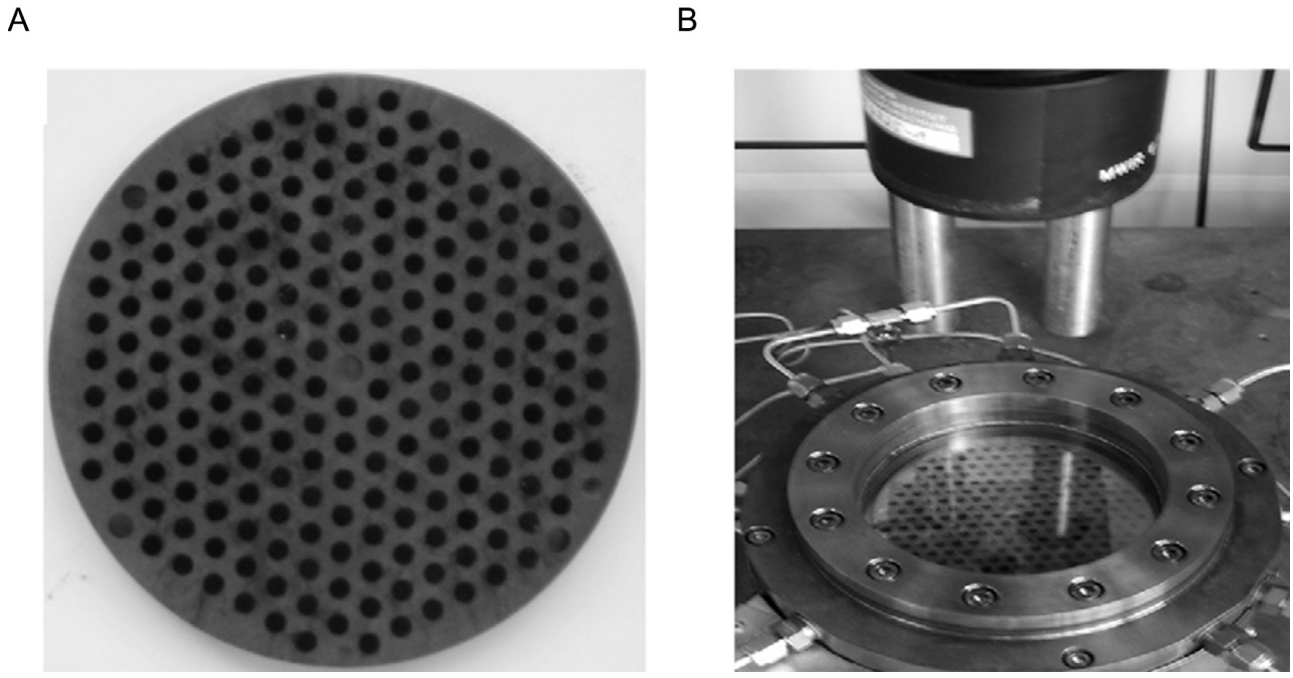

Fig. 12. A slate plate for catalyst–soot samples (Section A) and IR-camera and reactor with a catalyst library for IR-thermography (Section B). From Ref. [100].

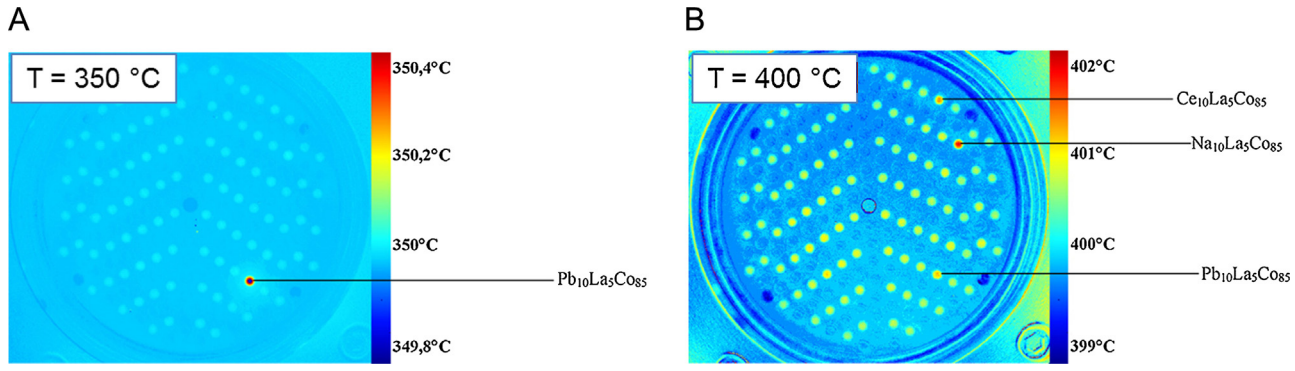

Fig. 13. The emissivity-corrected IR-thermographic image of catalyst library at 350 °C (Section A) and 400 °C (Section B) for soot combustion reaction. Adapted from Ref. [100].

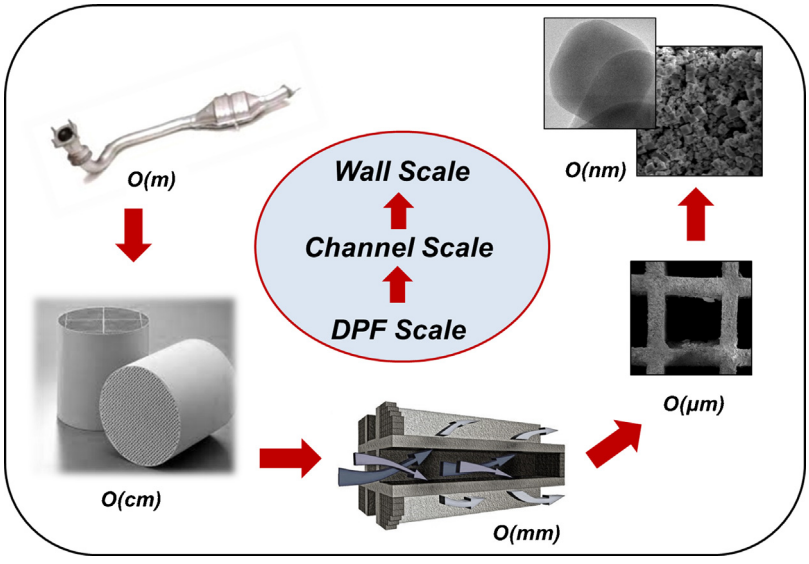

Fig. 14. The multiscale nature of a DPF. Adapted from Ref. [17].

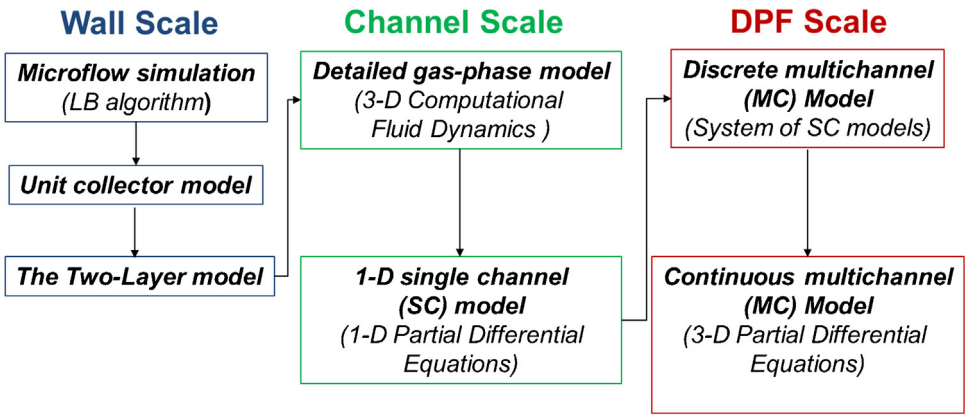

Fig. 15. The hierarchical structure of sub-models at the various spatial scales employed for DPF modelling. Adapted from Ref. [17].

scale, while dependence denotes information at a larger scale. This scheme reflects a trade-off of complexity at different scales of observation (=multiscale complexity). The multiscale nature of DPFs lends itself to a hierarchy of multiscale modelling of different spatial regimes. Hence, the models of each domain are classified according to their complexity and detail in the representation of the problem. As a whole, there are three coexisting length scales that need to be taken into account in the modelling of DPFs. The first scale (at the microscopic level) describes the phenomena that occur over the soot layer and the filter walls, the second one (at the single channel level) reflects the phenomena that take place along the filter channels, and the largest scale (at the macroscopic level) refers to the entire DPF. This means that three sub-models, corresponding to the different size scales (wall, channel, entire filter), can be combined to give an overall model of the filter, as schematized in Fig. 15.

From an analysis of the recent literature on such modelling efforts, the following issues can be highlighted:

- *At the smallest scale*, the only rigorous approach is the Lattice–Boltzmann (LB) algorithm applied to reconstructed microporous filter walls with discrete particle tracking [114], especially if the complexity of the catalyst–soot contact has to be fully understood in order to design new catalysts.
- *At the single channel level*, the most frequently studied case is definitely the 1-D PDE (Partial Differential Equations) single channel. Some of the critical features of the DPF performance can be seen at this scale, especially for the regeneration step (e.g., unevenness of the regeneration, dependence of the regeneration on the soot ignition strategy, etc.).
- *At the largest scale* (overall DPF canned in a pipe), continuous multichannel simulations are rare [115] because of the huge number of cells that have to be considered, although they are needed to a priori assess some uneven patterns of soot filtration and temperature profiles during regeneration, in order to differentiate the central channels from the peripheral ones;
- Over the last few years, several researchers have tried to simplify the modelling approaches at *two extreme scales* in order to make progress in the quest for a modelling tool to design new and higher performing traps, by exploiting:
  i) *The unit collector concept* [116]. This approach deals with the basic principles of the deep filtration process that takes place in the first filtration phases, until a soot cake is established. It is possible to take in account the effect of particle accumulation on the filtration process through the unit-cell-based filtration theory by extending it to include a local re-computation of the evolving unit-cell geometry caused by soot deposition. An example of the unit-cell filtration model is schematized in Fig. 16; the unit-cell is formed by a unit collector (diameter = d_c) and a "empty" envelope (diameter = b),which are matched to the macroscopic porosity of the filter. The unit-cell evolves over time, the size of the collector becomes a fraction of b,and a transient filtration model appears [116]. This approach leads to results that are in fair agreement with the experimental data. However, this method cannot be used to assess the nature of catalyst-soot contact.
  ii) *The Two-Layer model*. This approach was first proposed for soot over catalytically coated channel walls by Konstandopoulos et al. (vide supra) [116]. Similar approaches have also been developed by Serra et al. [35], and Ciambelli et al. [103], for TPC runs on catalyst-soot powder mixtures to highlight the presence of two combustion modes. The model is of a fitting type, and it can only be used for the "zone of catalyst influence". However, it does not provide any insight into the fundamentals of catalyst-soot contact or into the "migration" of oxidizing species (spillover effects).
  iii) *From 1-D to 3-D*. In an attempt to move from 1-D to 3-D modelling of the channel, Bensaid et al. [117,118] have shown that it is important to properly assess the uneven distribution of soot along the axial coordinate, a feature that is expected to have an important influence on the dynamics of the regeneration phase. Our research group has shown that at a 3-D channel level a Eulerian–Eulerian does not imply significant errors, compared to a Lagrangian–Eulerian approach [119], which requires a tremendous computational effort. It has also been observed that the design of the filter, as well as the feed section, can have a relevant impact on the soot accumulation pattern [120].

- Most of the modelling work done so far has been more of a *"single-shot" type* or, in the case of Konstandopoulos et al. [17] and Koltsakis et al. [121], of a continuous path type in which one step is added after another to model the current DPFs, but which does not prove a real tool to design or check new strategies. This was mentioned by Konstandopoulos when he said that, after about fifteen years of work in this field *"[. . .] from a research point of view, DPF simulation will focus on providing a deeper understanding and more detailed description of the coupled transport, structural and reaction micro-phenomena that occur at the wall and pore scales, to materialize the vision for an a priori design of advanced microstructures, hosting multifunctional catalysts for the highly compact and efficient emission control devices of the future"* [17]. Another example has been provided by Lee et al. [122] who, with the aim of optimizing filters as they are, analyzed the effect of the geometrical parameters (L/D, the cpsi, wall thickness, soot

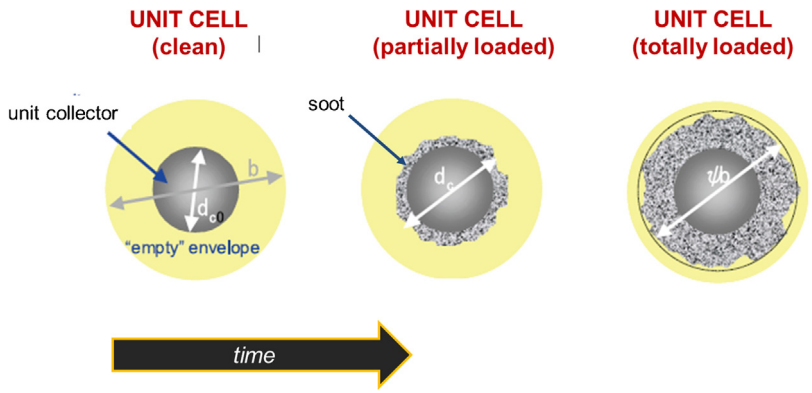

Fig. 16. Unit-cell filtration model. Adapted from Ref. [116b].

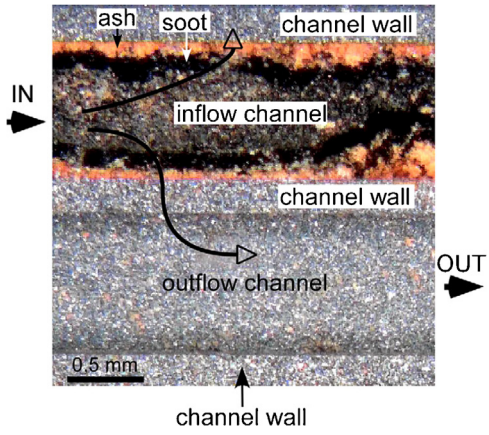

Fig. 17. Representative image of two neighboring (inflow–outflow) channels (Section parallel to the flow) showing the distribution of ash (reddish) and soot (black) at the outlet-mid part of DPF. Exhaust gas flows from the left to the right and is forced thorough the porous walls to the adjacent outflow channels. From Ref. [123].

loading), even under dynamic conditions, but failed to propose any trade-off or new design.

- One crucial aspect, in the case of Diesel exhaust treatment, is that of the *presence of ash*. A recent study [123] has shown that the problem of ash is paramount if one has to set up a "fit-for-life" multifunctional DPF with direct contact between the catalyst and soot. Ash in fact accumulates not only at the rear of the channels (where many studies on "fast regeneration" consider regeneration to start, e.g., [124–125]) but also on the channel walls. An example is illustrated in Fig. 17, in which two channels can be seen (section parallel to the flow) showing the distribution of ash (red) and soot (black) at the mid part of a DPF outlet [123]. Ash originates above all from the sulfur in the fuel, but also from the lubricants (S, Mg, Ca and Zn being the key components). There is no doubt that by lowering the sulfur content in the fuel, the problem will progressively be limited. It could also be expected that new, ashless lubricants could be developed. These seem to be prerequisites for the multifunctional trap concept to become a reality. However, it should be underlined that the process will not be driven by the potential development of a perfect catalytic trap itself.

  A pioneering study on ash deposition modelling was conducted by Deuschle et al. [126], even though it was more focused on the modelling of the fate of ash in time along the channels than on the specific issue of its interaction with a potential catalyst. The knowledge of ash deposition profiles inside the filter, and their impact on the pressure drop of the filter, are particularly important in regeneration strategies, which are based only on pressure drop: this signal could be misleading in identifying the correct soot loading to start filter regeneration.
- A key aspect that still needs to be taken into account for the modelling of DPFs is the necessity of moving *from a single particle size picture to include a size distribution effect*. This Eulerian–Eulerian approach, which was adopted by Toops et al. [109], is particularly interesting because it could easily be coupled to a population balance equation (PBE) for the description of poly-dispersed solid–gas flows, which would result in much lower computational costs than alternative Eulerian–Lagrangian approaches. In fact, a real soot distribution could be substituted by a series of mono-dispersed particle distributions, whose size and volume fraction could be calculated by means of a very efficient algorithm [127], and each of these populations could be treated as an independent dispersed phase, following the so-called "direct quadrature method of moments" [128]. These methods allow to know the proper soot deposition profile inside the filter and, ultimately, to select the most appropriate regeneration temperatures and strategies to avoid hot spots in the filter.
- Another important aspect is to move *from equivalent "spherical" soot particles* to *soot particles with fractal dimensions* [116], especially if the catalyst–soot contact conditions are to be predicted accurately. Konstandopoulos et al. [116] were the first to notice that the fractal structure of soot agglomerates provides "elastic" behavior to the soot cake, which is compressed at high GHSV values and returns to a more open structure when the engine starts to idle. Similarly, these Authors [129] have demonstrated that the morphology of the soot cake is influenced by the fractal nature of the soot, and the latter has a considerable influence on "mild" regeneration strategies. An important effect of the "elastic" behavior of soot cakes is that when high GHSV values are applied, the cake becomes compressed and the filtration efficiency is improved.

  Small soot particles are roughly spherical, but particles of approximately 100 nm (the most frequent in a Diesel soot distribution) are far from being spherical (fractal dimension >2), as can be shown in Fig. 18 [116]. However, a fractal dimensions >2 can also be observed for larger soot particles (up to 600 nm), thus showing the complex nature of soot generated by Diesel engines operating under different conditions.

  This is a crucial factor that needs to be taken into account in modelling and simulation, especially after the work of Yang et al. [130]. These Authors, using a very clever single-channel procedure, assessed the effect of the filtration properties of cordierite and SiC monoliths on ammonium sulfate particles generated by drying a solution aerosol. This method allows the particles to easily be washed away and a filtration run on a single filter to be restarted. Fig. 19 shows a schematic representation of the apparatus used by Yang et al. for the coating of a single wall DPF

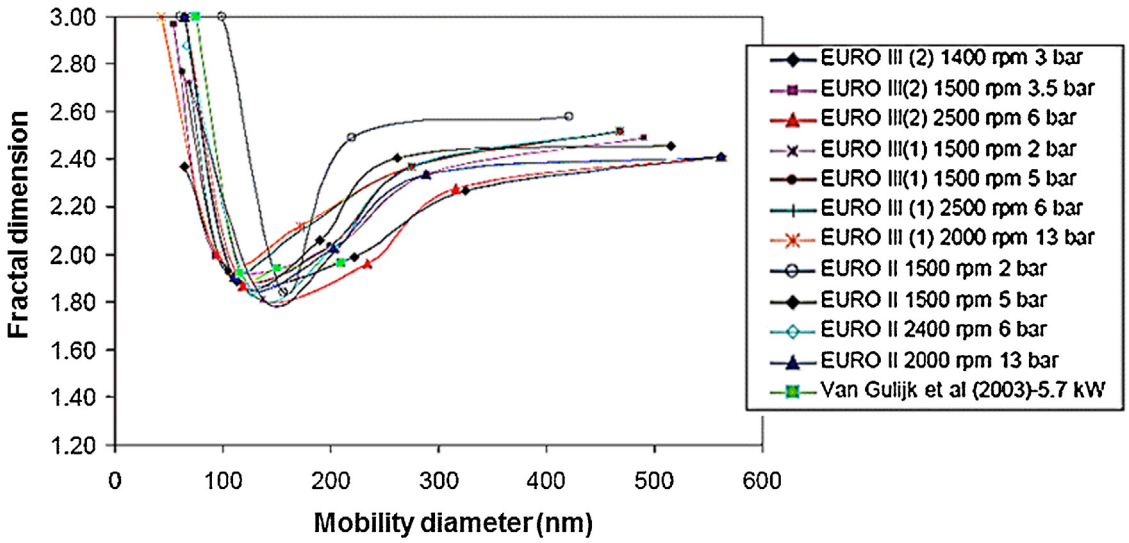

Fig. 18. Fractal dimension of soot aggregates with different mobility diameters obtained with different engines and operating conditions. Measurements from one Euro II and two Euro III Diesel engines and a Diesel generator. Adapted from Ref. [116c].

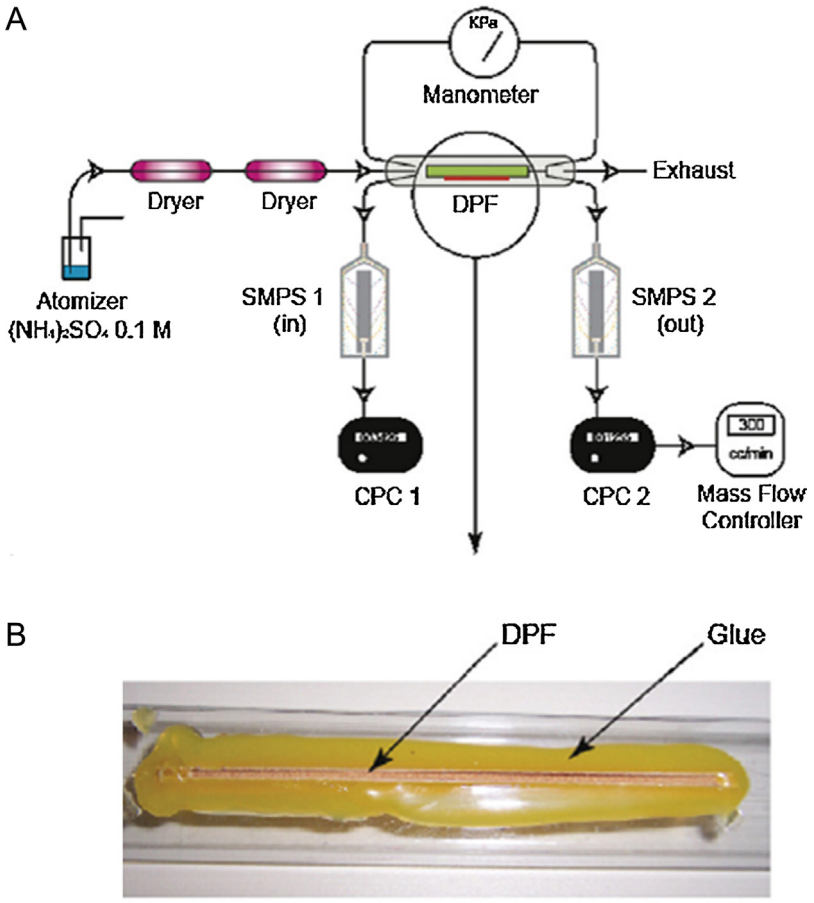

Fig. 19. Schematic representation of the experimental setup for coating single wall DPF with ammonium sulface particles (Section A). Picture of a single wall DPF glued to the central tube (Section B). Adapted from Ref. [130].

with $(NH_4)_2SO_4$ particles (Section A) as well as a photograph of the clear tube with an attached filter (Section B) [130]. Two scanning mobility particle sizers (SMPSs), and a condensation particle counter (CPC), were used to characterize the size distributions of the particles during the experiments. The Authors combined this experimental setup with an accurate filter characterization and with LB modelling, and showed that:

i) The filters are less efficient on soot particles in the 80–200 nm range, which is exactly the range in which soot particles would

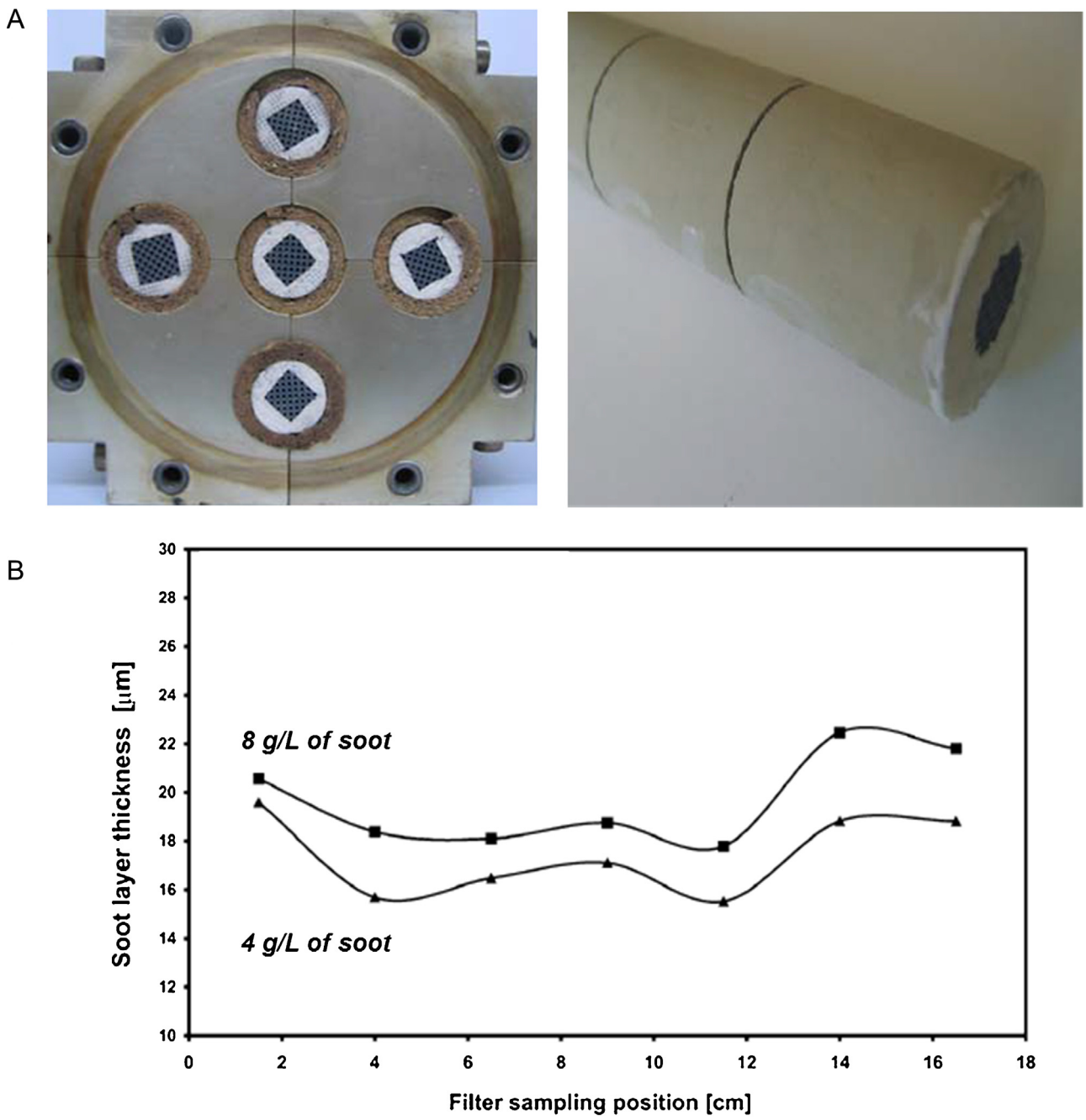

Fig. 20. DPF samples mounted inside the hosting module (left) and DPF sample preparation (right) (Section A); soot layer thickness profile along the DPF channel (Section B). Adapted from Ref. [131].

be less spherical; Brownian diffusion is very effective below 80 nm and interception is effective above 200 nm.

ii) The LB method that they have implemented, with some simplified assumptions, overestimates the filtration efficiencies, thus showing that a rigorous assumption is actually needed, without any simplifying factor.

iii) The interaction phenomenon with soot (and its fractal nature) may change, and for this reason the Authors are planning to test filters with real soot.

New test rigs and good filter characterization techniques are surely needed to validate the models. For instance, the above-mentioned Yang et al. model [130] needs to use 2 SMPS in parallel, one at the entrance and one at the outlet of the filter to obtain reliable data.

Fino et al. [131] were able to reconstruct the filtering media and quantify the soot loading profile well, without cutting the filter: small lab-scale DPF samples were loaded downstream from the Diesel oxidation catalyst (DOC) in an ad hoc designed reactor that is capable of housing five samples, with part of the entire flow produced by an automotive Diesel engine (Fig. 20A). Soot layer thickness was estimated by means of Field emission scanning electron microscope (FESEM) analysis after sample sectioning at progressive locations that were obtained through a procedure that had been defined to avoid affecting the distribution of the soot inside the filter and to enable the estimation of the actual soot thickness along the channel length (Fig. 20B).

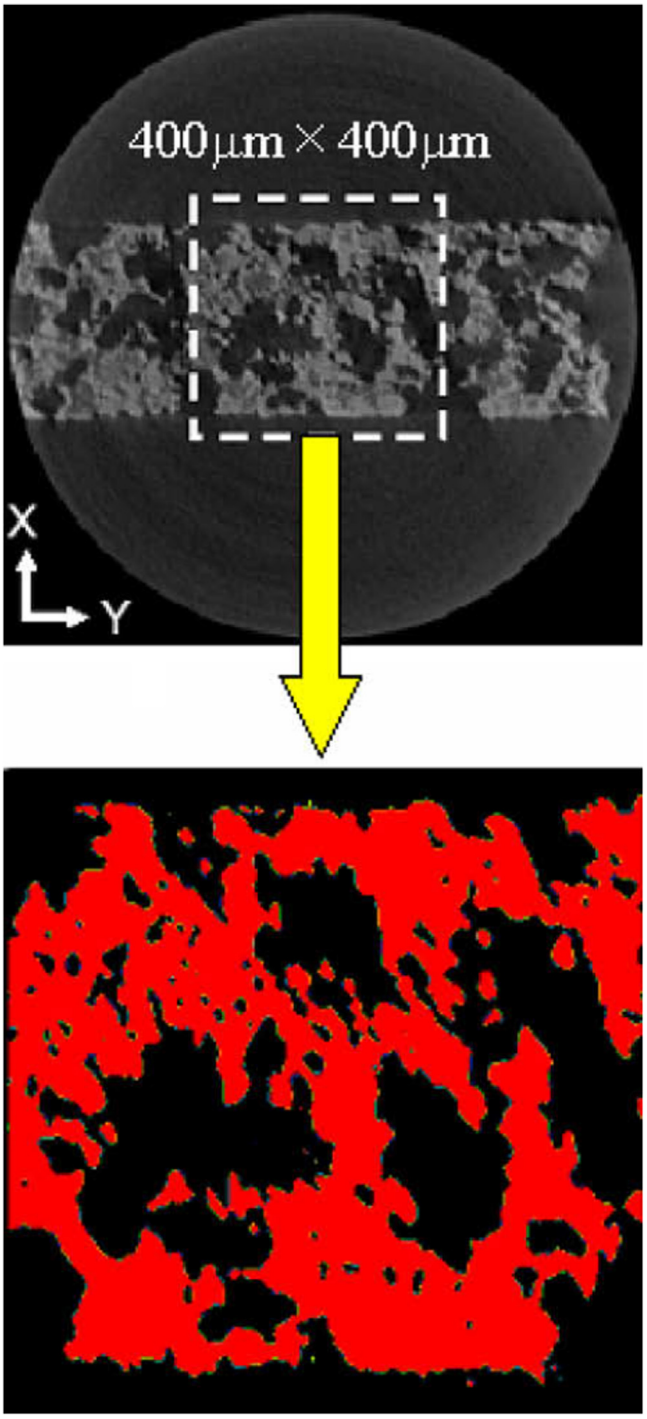

Fig. 21. Inner structure of DPF is obtained by X-ray CT technique. Upper figure shows the image area of the filter in x–y plane, and lower figure shows digitized data used in simulation. From Ref. [132].

Simulation of soot combustion and deposition in DPFs have been also achieved through the use of latest generation nano- and micro-tomography [132]. A side stream of research could arise from the work of Fischerauer et al. [133], who have demonstrated the general suitability of radiofrequency techniques for the determination of the soot content in Diesel particulate filters (in-situ). Fig. 21 shows a computer tomography (CT) image of the inner filter structure. The spatial resolution is 1 μm/pixel, which is the finest level in the reported CT measurements; the upper CT-image shows the image area of the filter in the x–y plane, whereas the lower CT-image shows the digitized data used in the simulation. It is possible to observe a complex porous framework with different pore sizes. Similarly, Fig. 22A shows the velocity field inside the filter, which is under a steady state with limited velocity perturbations (before soot deposition). Three different slice images are shown: (a) x = 40 μm, (b) x = 190 μm and (c) x = 340 μm. Fig. 22B shows the flow field and accumulated soot in the x–y plane at z = 32 μm (left) and in the y–z plane at x = 49 μm (right). These profiles are obtained at times = 104, 311 and 518 μs, respectively. However, these techniques might be more useful for control purposes than for filter characterization.

- A particular test rig is going to be assembled to follow regeneration conversely. It is based on an idea of Martirosyan et al. [134] in Houston. These Authors investigated the features of non-catalytic soot combustion. Fig. 23 shows temperature images corresponding to different combustion modes. In some cases, ignition occurs at a single point on the surface, creating a very hot region separated by sharp temperature fronts from the surrounding colder zones (Section A). The temperature fronts causes the hot zone to propagate both down-stream (in the flow direction) and upstream (opposite the flow direction) as well in the direction perpendicular to the flow. The high combustion rate in the hot zone leads to rapid soot combustion. However, ignition may occur at several different points on the DPF, and the ignited hot zones expand, due to the motion of the hot fronts. A typical thermal image is shown in Section B. The two black areas in that image are two locations at which the ignition has started, whereas the surrounding yellow hot zones are formed by collision of the moving fronts that originated from the ignition centers. Finally, the soot combustion proceeds uniformly at all the points on the planar DPF layer (Section C). It is worth noting that the combustion modes depend on the thickness soot layer. Indeed, Fig. 24 shows that for a thick soot layer (<150 μm), regeneration shifts from homogenous regeneration, characterized by infinite ignition points, to a finite number of ignition points, and finally to a single point for the thickest soot layers.

Most of the modelling done so far on regeneration is based on a 1-D approach [121]. However some particular characteristics should be noticed. For instance, Eigenberger et al. [124] stated that, in heterogeneous reactions, such as in a soot–gas system, the solid temperature profile inside a plug flow reactor is shaped according to the heat produced by the reaction rate in a slab, while the heat removed from the slab is shaped by the convective gas flow and solid axial conduction. These heats are either produced or removed at finite rates that can be different: if the thermal front (the speed of heat transported by convection and conduction) is slower than the reaction front (the speed at which the reaction advances in the axial direction), as soon as the solid attains the ignition temperature, it burns rapidly until it is locally consumed completely. An example of this is when the reaction rate is limited by solid depletion. Conversely, if the thermal front is faster than the reaction front, the local production of heat contributes to increase the solid temperature very rapidly, and favors the solid temperature homogenization in adjacent slabs. Another effect that could favor low reaction fronts, compared to thermal ones, would be oxygen depletion. If the two fronts have similar rates (i.e., the heat produced by soot combustion, at a certain axial position and in certain time steps, is enough to pre-heat and ignite the adjacent slab in the same time step), the temperature grows very rapidly, because the process is locally self-sustained and "confined", at least until one of the reactants becomes reaction-limiting.

A particular condition of a thermally-led reaction, is rear solid combustion in the plug flow, with ignition at the end. This is only possible in the case of the back-heating of the solid (conduction

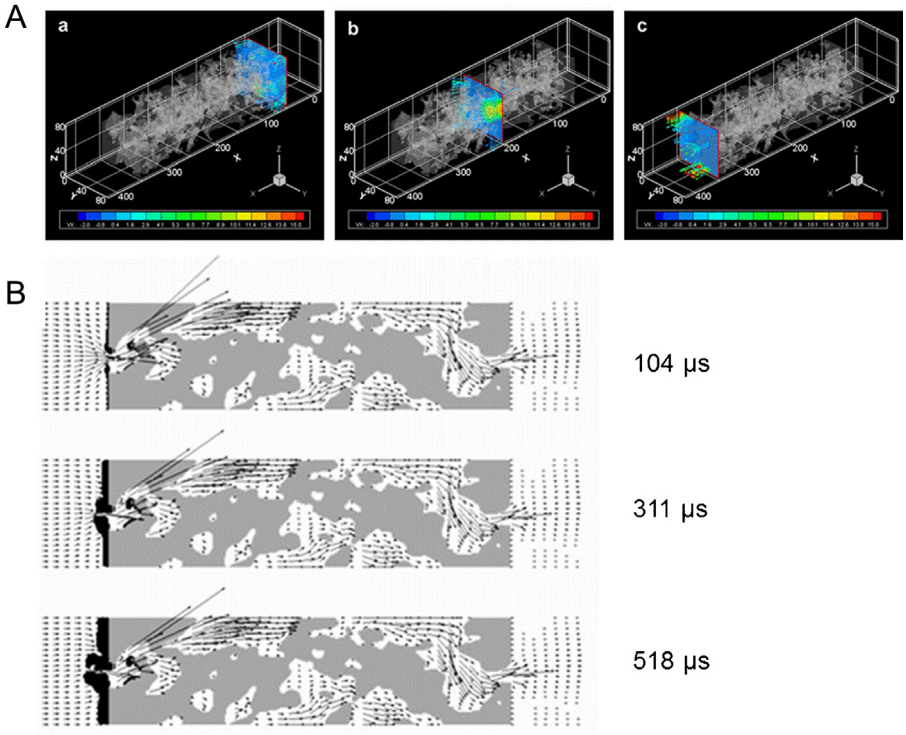

Fig. 22. Flow field and filter region shown by gray region; (a) $x = 40$ μm, (b) $x = 190$ μm, and (c) $x = 340$ μm (Section A); profiles of flow field and deposited soot in x–y plane at $z = 32$ μm. Adapted from Ref. [132].

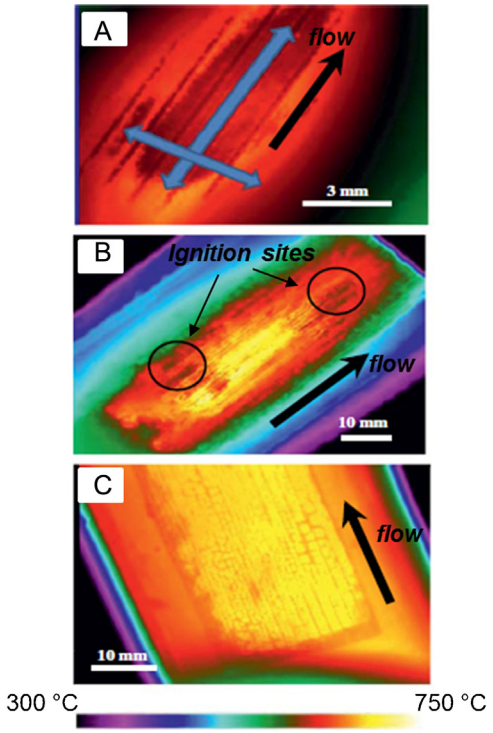

Fig. 23. Thermal images of soot regeneration during combustion by: (A) single ignition point; (B) two-ignition points and (C) uniform combustion. Adapted from Ref. [134].

minus convection, the latter being opposite the reaction front) and it is self-sustained only if the back-conducted heat produced by the reaction is higher than that removed by the convective flow.

In the case of soot oxidation within DPFs, the homogeneous reaction can be regarded as a condition in which the thermal front is faster than the reaction one, while fast regeneration occurs when the reaction is faster than the thermal front and the speed of the cake layer consumption is only physically limited by the soot cake thickness itself. A dangerous condition that should be avoided is that in which the reaction rate is very high and there is no O_2 depletion that could limit it. In this case, high flow rates must be used in order to avoid excessive temperatures and consequently the melting of the solid ceramic support (high flow rates have the effect of reducing the speed of the thermal front). In fact, very high temperatures are obtained when the thermal and the reaction fronts have approximately the same speed: the reaction propagates to the adjacent slab because it is self-sustained by thermal propagation and thus, temperature overshooting occurs. The data obtained by D. Luss in his experiments can most likely be explained on the grounds of these arguments.

- Along with the catalytic combustion of soot, the effect of oxidative fragmentation should be investigated in detail. Our group studied this aspect and discovered nanoparticles slip for very fast regeneration. A very active catalyst acts exactly where the slip occurs, by de-blocking the pores that had been plugged by soot in the early filtration stages, before the soot cake builds up and cake filtration starts. It has been shown, in Cauda et al. [135,136], that fast regeneration is detrimental to these advantages, when a catalyst appears in a highly foamy shape to favor the soot-catalyst contact.
- Studies on the optimal catalytic distribution in a trap should be made cautiously with any improved modelling tool. Some of the studies carried out so far can be considered doubtful, they provide conclusions that are too clear-cut, and they are based on rather weak assumptions. For instance, Bosch researchers [125] stated that a catalytic DPF with no DOC would only regenerate at the end of the channels, by means of HC conversion, which reaches a maximum at the rear end of the filter. Both the experimental data and operating conditions are reported in Fig. 25.

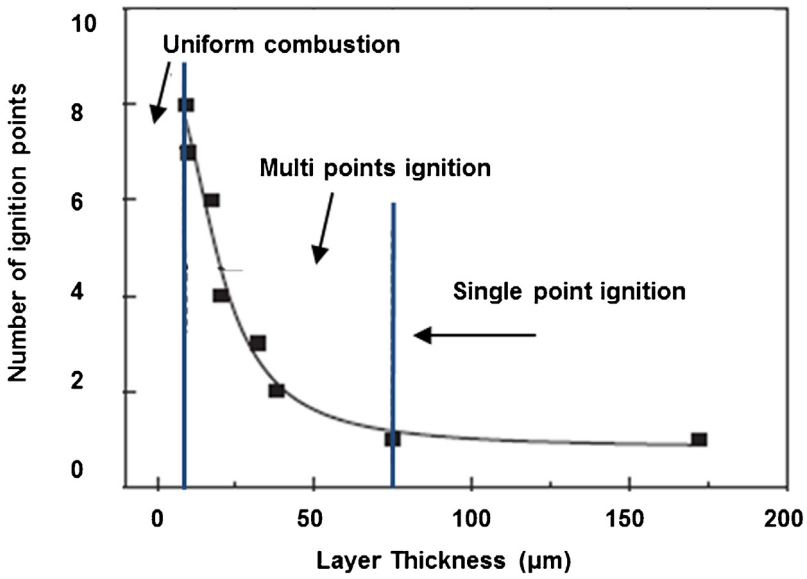

Fig. 24. Dependence of ignition points on PM layer thickness. Adapted from Ref. [134].

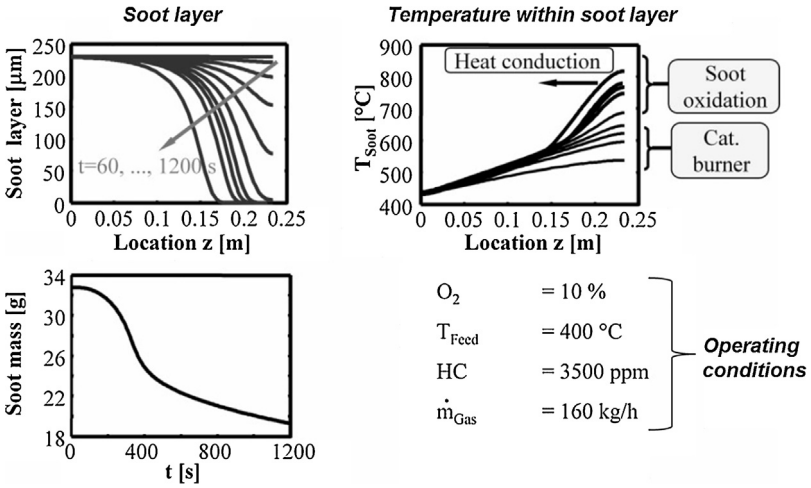

Fig. 25. Regeneration of a catalytic DPF initiated by HC conversion. Initial temperature = 400 °C. From Ref. [125].

- There is no doubt that, if the aim of a study is to examine a multifunctional catalytic trap, all the reactions and activity species have to be considered and the interferences between the functions should be outlined. The simultaneous removal of soot and NO_x in a single catalyzed filter (single brick solution) is the most ambitious strategy in this field, in view of the considerable advantages that would be attained in terms of both investment costs and pressure drop reduction. However, the dynamic behavior of soot–NO–O_2 reacting systems is very complex, and synergistic effects may arise in the active sites of multicomponent catalysts [39].

9. Conclusions

The current soot oxidation catalyst scenario has been reviewed briefly, highlighting both the kinetic aspects of soot combustion and the main factors that affect the activity of powder catalysts. Different experimental conditions may be found in literature, and hence the comparison of catalyst activities measured in different laboratories remains a fundamental problem. In recent years, many soot oxidation catalysts have been investigated and the most recent catalytic technologies focus on stable materials that exhibit high mobility of the oxidizing species.

It has been shown that active sites are not static at solid surfaces and may interact with each other through transport phenomena and surface flexibility. As a whole, the dynamic behavior of DPF systems is very complex, due to the nonlinear interplay of the reaction kinetics, the presence of different functionalities assembled on the same monolithic support (catalysis and filtration), the transfer phenomena and the operating conditions that vary over time. Nevertheless, the stability of soot combustion catalysts is fundamental for application of catalytic materials in DPFs and hence accelerated deactivation procedures are necessary to evaluate possible candidates.

Several DPF modelling and simulation approaches have been developed in order to investigate a wide range of experimental conditions, for optimization purposes. The multiscale nature of DPFs lends itself to a hierarchical organization of models, across various orders of magnitude (from the atomic regime to the macroscale). These sub-models are usually classified according to their complexity and detail in the representation of the phenomena, and are combined to give an overall model. Different observation scales (e.g., wall, channel, entire filter) have often been addressed with

separate modelling approaches but they have rarely been connected to one another, mainly because of computational problems. However, catalytic traps exhibit an intrinsic multiscale complexity, which is reflected by a trade-off between fine and large-scale phenomena. Consequently, the behavior of multifunctional traps usually results in a non-linear combination of transport and kinetic factors that are therefore different from a sum of the elementary phenomena. This means that new modelling approaches will be necessary to correctly and simultaneously compute the performance of catalytic traps. On the catalytic material side, new challenges would be addressed towards the synthesis of multicomponent catalysts based on a combination of metal oxides and, on the other hand, the modification of the structural parameters via the design of advanced nanoshapes, which can lead to interesting physico-chemical properties. Many solid catalysts, that are now widely applied in automotive technology, have been designed in an empirical way. However, improvements of these catalysts, with resulting benefits to catalytic activity, have derived from the recent development of in-situ characterization techniques, molecular modelling and novel synthesis procedures. Such a trend should continue in the future with the new generations of scientists and engineers.

Acknowledgment

The Ministero dell'Università e della Ricerca (MIUR) (grant number: RBFR12LS6M 001) is acknowledged for sponsoring this research activity (FIRB—Futuro in Ricerca 2012).

References

[1] E. Aneggi, C. de Leitenburg, A. Trovarelli, in: A. Trovarelli, P. Fornasiero (Eds.), Catalysis by Ceria and Related Materials, 2nd ed., Imperial College Press, London, 2013, pp. 565–621.
[2] R.M. Heck, R.J. Farrauto, S.T. Gulati, Catalytic Air Pollution Control: Commercial Technology, 3rd ed., Wiley-VCH, Hoboken, New Jersey, 2006, pp. 518.
[3] E.S.J. Lox, in: G. Ertl, H. Knözinger, F. Schüth, J. Weitkamp (Eds.), Handbook of Heterogeneous Catalysis, 2nd ed., Wiley-VCH, Weinheim, 2008, pp. 2274–2344.
[4] B. Frank, R. Schlögl, D.S. Su, Environ. Sci. Technol. 47 (2013) 3026–3027.
[5] http://www.eea.europa.eu/media/newsreleases/reducing-the-20ac-45-billion.
[6] A. Bueno-López, Appl. Catal. B 146 (2014) 1–11.
[7] Burch, Catal. Rev. 46 (2004) 271–334.
[8] A. Russell, W.S. Epling, Catal. Rev. Sci. Eng. 53 (2011) 337–423.
[9] P. Eastwood, Critical Topics in Exhaust Gas Aftertreatment, Research Studies Press Ltd., Baldock, England, 2000, pp. 400.
[10] J. Oi-Uchisawa, A. Obuchi, S. Wang, T. Nanba, A. Ohi, Appl. Catal. B 43 (2003) 117–129.
[11] C.A. Neyertz, E.D. Banus, E.E. Miró, C.A. Querini, Chem. Eng. J. 248 (2014) 394–405.
[12] I. Atribak, F.E. Lopez-Suarez, A. Bueno-Lopez, A. Garcia-Garcia, Catal. Today 176 (2011) 404–408.
[13] S. Bensaid, N. Russo, D. Fino, Catal. Today 216 (2013) 57–63.
[14] D. Fino, Sci. Technol. Adv. Mater. 8 (2007) 93–100.
[15] D. Fino, P. Fino, G. Saracco, V. Specchia, Chem. Eng. Sci. 58 (2003) 951–958.
[16] D. Chatterjee, V. Schmeißer, M. Frey, M. Weibel, in: O. Deutschmann (Ed.), Modeling and Simulation of Heterogeneous Catalytic Reactions, Weinheim, Wiley-VCH, 2012, pp. 303–331.
[17] A.G. Konstandopoulos, M. Kostoglou, N. Vlachos, Int. J. Veh. Des. 41 (2006) 256–284.
[18] I. Atribak, A. Bueno-López, A. García-García, Comb. Flame 157 (2010) 2086–2094.
[19] J. Uchisawa, A. Obuchi, T. Nanba, in: D. Duprez, F. Cavani (Eds.), Handbook of Advanced Methods and Processes in Oxidation Catalysis, Imperial College Press, 2014, pp. 25–50.
[20] P.A. Neeft, M. Makkee, J.A. Moulijn, Appl. Catal. B 8 (1996) 57–78.
[21] M. Piumetti, S. Bensaid, N. Russo, D. Fino, Appl. Catal. B 165 (2015) 742–751.
[22] P. Miceli, S. Bensaid, N. Russo, D. Fino, Nanoscale Res. Lett. 9 (2014) 254.
[23] S. Bensaid, G.A. Blengini, D. Fino, N. Russo, Chem. Eng. Commun. 201 (2014) 1327–1339.
[24] P.A. Kumar, M.D. Tanwar, S. Bensaid, N. Russo, D. Fino, Chem. Eng. J. 207 (2012) 258–266.
[25] M. Issa, H. Mahzoul, A. Brillard, J.-F. Brilhac, Chem. Eng. Technol. 3 (2009) 1859–1865.
[26] S. Bensaid, E. Merlone Borla, N. Russo, D. Fino, V. Specchia, Ind. Eng. Chem. Res. 49 (2010) 10323–10333.
[27] J.C. Védrine, Appl. Catal. A 474 (2014) 40–50.
[28] J.C. Freund, Chem. Eur. J. 16 (2010) 9384–9397.
[29] G. Ertl, Angew Chem. Int. Ed. Engl. 29 (1990) 1219–1227.
[30] G. Ertl, Angew. Chem. Int. Ed. 47 (2008) 3524–3535.
[31] L. Castoldi, R. Matarrese, L. Lietti, P. Forzatti, Appl. Catal. B 90 (2009) 278–285.
[32] P. Legutko, W. Kaspera, T. Jakubek, P. Stelmachowski, A. Kotarba, Top. Catal. 56 (2013) 745–749.
[33] Y. Watabe, K. Yrako, T. Miyajima, T. Yoshimoto, Y. Murakami, SAE Paper 830082 (1983).
[34] D. Fino, N. Russo, C. Badini, G. Saracco, V. Specchia, AICHE J. 49 (2003) 2173–2180.
[35] V. Serra, G. Saracco, C. Badini, V. Specchia, Appl. Catal. B 11 (1997) 329–346.
[36] A. Setiabudi, M. Makkee, J.A. Moulijn, Appl. Catal. B 50 (2004) 185–194.
[37] D. Fino, N. Russo, G. Saracco, V. Specchia, J. Catal. 217 (2003) 367–375.
[38] A. Bueno López, K. Krishna, M. Makkee, J.A. Moulijn, Catal. Lett. 99 (2005) 203–205.
[39] L.T. Weng, B. Delmon, Appl. Catal. A 81 (1992) 141–213.
[40] J. Neeft, T.X. Nijhuis, E. Smakman, M. Makkee, J. Moulijn, Fuel 76 (1997) 1129–1136.
[41] A. Yezerets, N.W. Currier, D.H. Heui Kim, H.A. Eadler, W.S. Epling, C.H.F. Peden, Appl. Catal. B 61 (2005) 120–129.
[42] A. Messerer, R. Niessner, U. Poschl, Carbon 44 (2006) 307–324.
[43] C.J. Tighe, M.V. Twigg, A.N. Hayhurst, J.S. Dennis, Combust. Flame 159 (2012) 77–90.
[44] N. Zouaoui, M. Labaki, M. Jeguirim, C.R. Chimie 17 (2014) 672–680.
[45] M. Jeguirim, V. Tschamber, P. Lehrburger, Appl. Catal. B 76 (2007) 235–240.
[46] I. Atribak, A. Bueno-López, A. García-García, Catal. Commun. 9 (2008) 250–255.
[47] B. Azambre, S. Collura, P. Darcy, J.M. Trichard, P. Da Costa, A. García-García, A. Bueno-López, Fuel Process. Technol. 92 (2011) 363–371.
[48] W. Guo, H. Xiao, E. Yasuda, Y. Cheng, Carbon 44 (2006) 3269–3276.
[49] W. Guo, H. Xiao, Carbon 45 (2007) 1058–1065.
[50] P. Darcy, P. Da Costa, H. Mellottée, J.M. Trichard, G. Djéga-Mariadassou, Catal. Today 119 (2007) 252–256.
[51] M.S. Gross, M.A. Ulla, C.A. Querini, Appl. Catal. A 360 (2009) 81–88.
[52] K. Krishna, A. Bueno-López, M. Makkee, J.A. Moulijn, Appl. Catal. B 75 (2007) 189–200.
[53] A. Bueno-López, K. Krishna, M. Makkee, J.A. Moulijn, J. Catal. 230 (2005) 237–248.
[54] A. Bueno-López, K. Krishna, B. van der Linden, G. Mul, J.A. Moulijn, M. Makkee, Catal. Today 121 (2007) 237–245.
[55] P. Darcy, P. Da Costa, H. Mellottée, J.M. Trichard, G. Djéga-Mariadassou, Catal. Today 119 (2007) 252–256.
[56] M. Machida, Y. Murata, K. Kishikawa, D. Zhang, K. Ikeue, Chem. Mater. 20 (2008) 4489–4494.
[57] L. Zhu, J. Yu, X. Wang, J. Hazard. Mater. 140 (2007) 205–210.
[58] M.N. Bokova, C. Decarne, E. Abi-Aad, A.N. Pryakhin, V.V. Lunin, A. Aboukaïs, Thermochim. Acta 428 (2005) 165–171.
[59] K. Shimizu, H. Kawachi, A. Satsuma, Appl. Catal. B 96 (2010) 169–175.
[60] G. Kastrinaki, S. Lorentzou, A.G. Konstandopoulos, Emiss. Control Sci. Technnol. 1 (2015) 247–253.
[61] M.S. Gross, M.A. Ulla, C.A. Querini, J. Mol. Catal. A: Chem. 352 (2012) 86–94.
[62] M.S. Gross, B.S. Sánchez, C.A. Querini, Chem. Eng. J. 168 (2011) 413–419.
[63] N. Labhsetwar, R.B. Biniwale, R. Kumar, S. Devotta, Catal. Surv. Asia 10 (2006) 55–64.
[64] E. Aneggi, D. Wiater, C. de Leitenburg, J. Llorca, A. Trovarelli, ACS Catal. 4 (2014) 172–181.
[65] G. Busca, Heterogeneous Catalytic Materials, Amsterdam, Elsevier, 2014, pp. 375–412.
[66] E. Aneggi, C. de Leitenburg, A. Trovarelli, Catal. Today 181 (2012) 108–115.
[67] E. Aneggi, M. Boaro, C. de Leitenburg, G. Dolcetti, A. Trovarelli, J. Alloys Compd. 408–412 (2006) 1096–1102.
[68] S. Bernal, G. Blanco, J.M. Pintado, J.M. Rodrìguez-Izquierdo, M.P. Yeste, Catal. Commun. 6 (2005) 582–585.
[69] S. Carrettin, P. Concepción, A. Corma, J.M. López-Nieto, V.F. Puntes, Angew. Chem. Int. Ed. 43 (2004) 2538–2540.
[70] N. Guillén-Hurtado, A. García-García, A. Bueno-López, Appl. Catal. B 174–175 (2015) 60–66.
[71] S.J. Tans, A.R.M. Verschueren, C. Dekker, Nature 393 (1998) 49–52.
[72] S.S. Fan, M.G. Chapline, N.R. Franklin, T.W. Tombler, A.M. Cassell, H. Dai, Science 283 (1999) 512–514.
[73] A.K. Geim, K.S. Novoselov, Nat. Mater. 3 (2007) 183–191.
[74] D.L. Feldheim, C.A. Foss, in: D.L. Feldheim, C.A. Foss (Eds.), Metal Nanoparticles: Synthesis, Characterization and Applications, Marcel Dakker, New York, 2002, pp. 1–16.
[75] J.M. Thomas, R. Raja, Top. Catal. 53 (2010) 848–858.
[76] S. Chowdhury, K.-S. Lin, J. Nanomater. 2011 (2011) 1–16.
[77] N. Ta, J. Liu, S. Chenna, P.A. Crozier, Y. Li, A. Chen, W.J. Shen, J. Am. Chem. Soc. 134 (2012) 20585–20588.
[78] Z.L. Wu, M.J. Li, S.H. Overbury, J. Catal. 285 (2012) 61–73.
[79] X. Du, D. Zhang, L. Shi, R. Gao, J. Zhang, J. Phys. Chem. C 116 (2012) 10009–10016.

[80] Y. Wei, Z. Zhao, X. Yu, B. Jin, J. Liu, C. Xu, A. Duan, G. Jiang, S. Ma, Catal. Sci. Technol. 3 (11) (2013) 2958–2970.
[81] L. Shuang, W.U. Xiaodong, W. Duan, R. Rui, J. Rare Earths 33 (6) (2015) 567–589.
[82] M. Piumetti, S. Bensaid, N. Russo, D. Fino, Appl. Catal. B 180 (2016) 271–282.
[83] N. Labhsetwar, M. Dhakad, S.S. Rayalu, R. Kumar, J. Subrt, H. Haneda, S. Devotta, T. Mitsuhashi, Top. Catal. 42–43 (2007) 299–302.
[84] P. Doggali, H. Kusaba, S. Rayalu, Y. Teraoka, N. Labhsetwar, Top. Catal. 56 (2013) 457–461.
[85] J. Zhu, A. Thomas, Appl. Catal. B 92 (2009) 225–233.
[86] C.H. Kim, G. Qi, K. Dahlberg, W. Li, Science 327 (2010) 1624–1627.
[87] Q. Li, M. Meng, N. Tsubaki, X. Li, Z. Li, Y. Xie, T. Hu, J. Zhang, Appl. Catal. B 91 (2009) 406–415.
[88] Q. Li, M. Meng, Z.Q. Zou, X.G. Li, Y.Q. Zha, J. Hazard. Mater. 161 (2009) 366–372.
[89] B. Ura, J. Trawczynski, A. Kotarba, W. Bieniasz, M.J. Illá-Gómez, Appl. Catal. B 101 (2011) 169–175.
[90] H. Lin, Y. Li, W. Shangguan, Z. Huang, Combust. Flame 156 (2009) 2063–2070.
[91] D. Fino, N. Russo, E. Cauda, G. Saracco, V. Specchia, Catal. Today 114 (2006) 31–39.
[92] T. Hirano, T. Tosho, T. Watanabe, T. Akiyama, J. Alloys Compd. 470 (2009) 245–249.
[93] G. Zhang, Z. Zhao, J. Liu, J. Xu, Y. Jing, A. Duan, G. Jiang, J. Rare Earths 27 (2009) 955–960.
[94] S. Li, R. Kato, Q. Wang, T. Yamanaka, T. Takeguchi, W. Ueda, Appl. Catal. B 93 (2010) 383–386.
[95] S. Furfori, S. Bensaid, N. Russo, D. Fino, Chem. Eng. J. 154 (2009) 348–354.
[96] S. Furfori, N. Russo, D. Fino, G. Saracco, V. Specchia, Chem. Eng. Sci. 65 (2010) 120–127.
[97] E. Ambroise, C. Courson, A. Kiennemann, A.-C. Roger, O. Pajot, E. Samson, G. Blanchard, Top. Catal. 52 (2009) 2101–2107.
[98] S. Bensaid, N. Russo, Catal. Today 176 (2011) 417–423.
[99] B.S. Sánchez, C.A. Querini, E.E. Miró, Appl. Catal. A 366 (2009) 166–175.
[100] N.E. Olong, K. Stöwe, W.F. Maier, Catal. Today 137 (2008) 110–118.
[101] X. Zhou, H. Chen, G. Zhang, J. Wang, Z. Xie, Z. Hua, L. Zhang, J. Shi, J. Mater. Chem. A 3 (2015) 9745–9753.
[102] S. Lorentzou, C. Pagkoura, E. Papaioannou, M. Kostoglou, A.G. Konstandopoulos, K. Ohno, K. Ogyu, T. Oya, 3rd European Combustion Meeting, Chania-Crete, 2007.
[103] P. Ciambelli, P. Corbo, M. Gambino, V. Palma, S. Vaccaro, Catal. Today 27 (1996) 99–106.
[104] H. Jansma, D. Fino, R. Uitz, M. Makkee, Ind. Eng. Chem. Res. 51 (2012) 7559–7564.
[105] B.A.A.L. van Setten, R. van Dijk, S.J. Jelles, M. Makkee, J.A. Moulijn, Appl. Catal. B 21 (1999) 51–61.
[106] A. Setiabudi, N.K. Allaart, M. Makkee, J.A. Moulijn, Appl. Catal. B 60 (2005) 233–243.
[107] R.A. Yapaulo, E. Wirojsakunchai, T. Orita, D.E. Foster, M. Akard, L.R. Walker, M.J. Lance, Int. J. Engine Res. 10 (2009) 287–304.
[108] M. Issa, C. Petit, H. Mahzoul, A. Aboukaïs, J.F. Brilhac, Top. Catal. 52 (2009) 2063–2069.
[109] T.J. Toops, J.A. Pihl, C.E.A. Finney, J. Gregor, H. Bilheux, Emiss. Control Sci. Technol. 1 (2015) 24–31.
[110] J.C. Caroca, F. Millo, D. Vezza, T. Vlachos, A. De Filippo, S. Bensaid, N. Russo, D. Fino, Ind. Eng. Chem. Res. 50 (2011) 2650–2658.
[111] E.E. Iojoiu, B. Bassoua, G. Nolven, D. Farrusseng, A. Smartin Chomel, K. Lombaert, D. Bianchi, C. Mirodatos, Catal. Today 137 (2008) 103–109.
[112] M. Ambrogio, G. Saracco, V. Specchia, C. van Gulijk, M. Makkee, J.A. Moulijn, Sep. Purif. Technol. 27 (2002) 195–209.
[113] H.M. Reichenbach, A. Hongmei, P.J. McGinn, Appl. Catal. B 44 (2003) 347–354.
[114] M.J. Biggs, S.J. Humby, A. Buts, U. Tüzün, Chem. Eng. Sci. 58 (2003) 1271–1288.
[115] M. Kostoglou, P. Housiada, A.G. Konstandopoulos, Chem. Eng. Sci. 58 (2003) 3273–3283.
[116] (a) A.G. Konstandopoulos, E. Papaioannou, KONA Powder Particle J. 26 (2008) 36–65;
(b) C. Van Gulijk, J.C.M. Marijnissen, M. Makkee, J.A. Moulijn, A. Schmidt, J. Aero. Sci. 35 (2004) 633–655;
(c) A.G. Konstandopoulos, M. Kostoglou, E. Skaperdas, E. Papaioannou, D. Zarvalis, E. Kladopoulou, SAE Tech. Paper, 2000-01-2016; SAE Trans. 109 (2000) 683-705; SAE SP, 1497 in: Diesel Exhaust Aftertreatment (2000) 189-211.;
(d) N. Vlachos, P. Housiada, D. Zarvalis, A.G. Konstandopoulos, In: Particle Loading & Filtration Kinetis in Fibrous Filters, U. Karlsruhe (2002).
[117] S. Bensaid, D.L. Marchisio, D. Fino, G. Saracco, V. Specchia, Chem. Eng. J. 154 (2009) 211–218.
[118] S. Bensaid, D.L. Marchisio, D. Fino, Chem. Eng. Sci. 65 (2010) 357–363.
[119] F. Sbrizzai, P. Faraldi, A. Soldati, Chem. Eng. Sci. 60 (2005) 6551–6563.
[120] S. Bensaid, D.L. Marchisio, N. Russo, D. Fino, Catal. Today 147S (2009) S295–S300.
[121] G.C. Koltsakis, A.M. Stamatelos, Ind. Eng. Chem. Res. 36 (1997) 4155–4165.
[122] S.J. Lee, S.J. Jeong, W.S. Kim, Appl. Energy 86 (2009) 1124–1135.
[123] A. Liati, P.D. Eggenschwiler, Combust. Flame 159 (2010) 1658–1670.
[124] G. Eigenberger, G. Kolios, U. Nieken, Chem. Eng. Sci. 62 (2007) 4825–4841.
[125] R. Peck, C. Becker, Chem. Eng. Technol. 32 (2009) 1411–1422.
[126] T. Deuschle, U. Janoske, M. Piesche, Chem. Eng. J. 135 (2008) 49–55.
[127] R.O. Fox, in: D.L. Marchisio, R.O. Fox (Eds.), Multiphase Reacting Flows: Modelling and Simulation, vol. 492, Springer Verlag, 2007, 2015, pp. 1–40.
[128] D.L. Marchisio, R.O. Fox, J. Aerosol Sci. 36 (2005) 43–73.
[129] M. Kostoglou, A.G. Konstandopoulos, AIChE J. 51 (2005) 2534–2546.
[130] J. Yang, M. Stewart, G. Maupin, D. Herling, A. Zelenyuk, Chem. Eng. Sci. 64 (2009) 1625–1634.
[131] D. Fino, N. Russo, F. Millo, D.S. Vezza, F. Ferrero, F. Chianale, Top. Catal. 52 (2009) 2083–2087.
[132] K. Yamamoto, S. Oohori, H. Yamashita, S. Daido, Proc. Combust. Inst. 32 (2009) 1965–1972.
[133] G. Fischerauer, M. Förster, R. Moos, Meas. Sci. Technol. 21 (2010) 1–6.
[134] K.S. Martirosyan, K. Chen, D. Luss, Chem. Eng. Sci. 65 (2010) 42–46.
[135] E. Cauda, S. Hernandez, D. Fino, G. Saracco, V. Specchia, Environ. Sci. Technol. 40 (2006) 5532–5537.
[136] E. Cauda, S. Hernandez, D. Fino, G. Saracco, V. Specchia, Top. Catal. 42–43 (2007) 253–257.